disease or an autoinflammatory disease [1–3]. Approximately 50 % of aHUS patients have been reported to have mutations in the genes coding for regulators or components of the complement alternative pathway, complement factor H (*CFH*), complement factor H-related 5, complement factor I (*CFI*), membrane cofactor protein (*MCP*), complement factor B (*CFB*), complement component 3 (*C3*) and thrombomodulin (*THBD*) [1, 4, 5]. In particular, *CFB* mutations in aHUS patients are extremely rare [1, 6–10], accounting for 0 to 3 % of aHUS patients [1, 4], and are only noted marginally in updated classifications of primary immunodeficiency diseases [2].

To further understand aHUS associated with a *CFB* mutation, we analyzed a large kindred with aHUS associated with a *CFB* missense mutation (c.1050G>C, p.Lys350Asn) in exon 8.

Methods

Patients

The pedigree of a nonconsanguineous Japanese kindred that we studied is depicted in Fig. 1a, and a summary of the clinical and laboratory data of 3 members with aHUS is given in Table I.

DNA Sequencing

Genomic DNA was extracted from leukocytes using SepaGene (Eidia, Tokyo, Japan). DNA fragments of the *CFH*, *CFI*, *MCP*, *CFB*, *C3*, and *THBD* were amplified by PCR and analyzed using Big Dye Terminator Bidirectional Sequencing (Applied

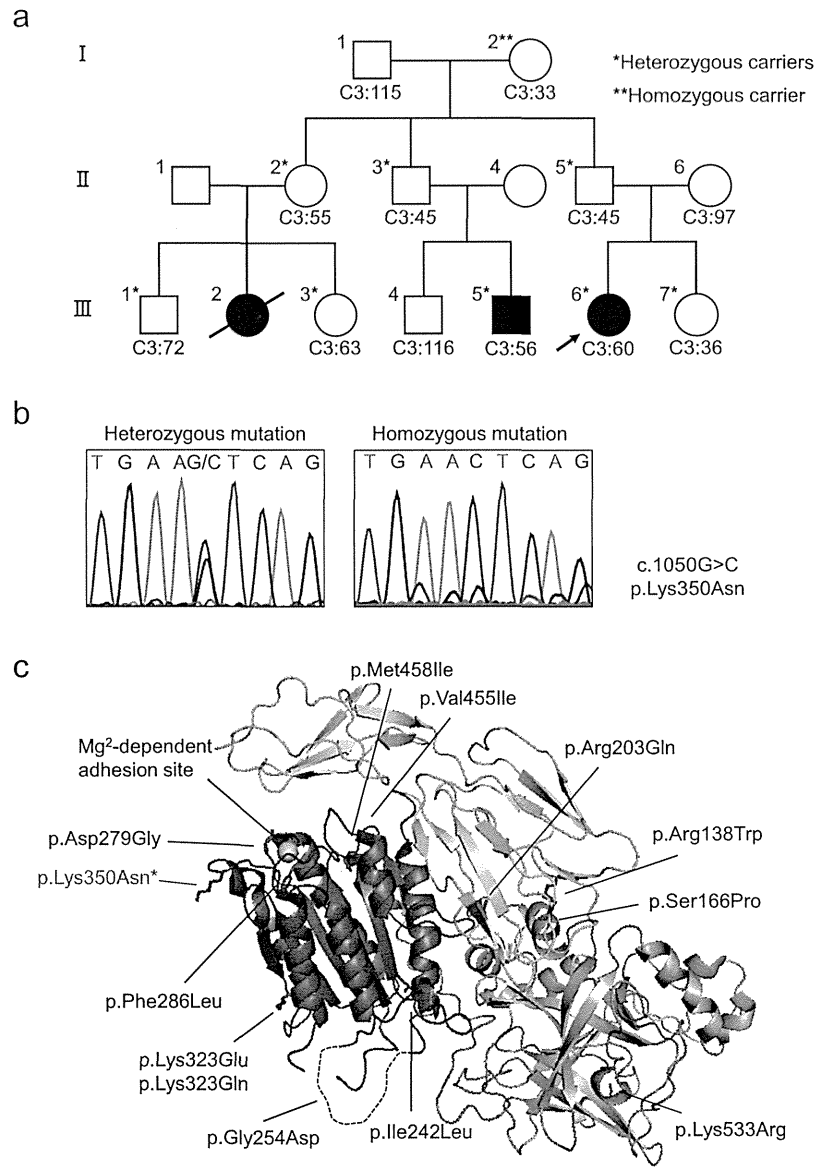

Fig. 1 **a**, Pedigree of kindred we studied. Individuals are identified by numbers within each generation. Arrow indicates the proband. Black and white symbols indicate, respectively, affected and unaffected individuals. One deceased individual is crossed. Heterozygous mutation carriers are indicated by asterisks, and one homozygous mutation carrier by double asterisks. Serum C3 levels (mg/dl) in a normal situation are shown below symbols **b**, Genetic analysis of the *CFB* **c**, Structures of the von Willebrand type A (VWA) domain (blue), the serine protease (SP) domain (green), and three complement-control protein (CCP) domains (yellow) in CFB. The location of the mutation we identified (*) and previously reported mutations are shown

Table I Clinical characteristics and laboratory data on admission of aHUS patients

	Patient III-2	Patient III-5	Patient III-6	Normal values
Onset (year)	1998	2010	2007	
Onset age (months)	8	6	20	
Gender	Female	Male	Female	
Extrarenal manifestations	No	No	No	
Chief complaint	Vomiting	Rhinorrhea	Cough	
	Fever	Fever	Fever	
	Paleness	Paleness	Paleness	
Diarrhea	Negative	Negative	Negative	
Hemoglobin (g/dl)	4.7	5.9	6.9	9.0–13.0
Platelet (/μl)	99,000	54,000	71,000	200,000–250,000
LDH (IU/l)	1,121	2,285	2,359	235–335
BUN (mg/dl)	72.6	53.0	96.6	10.0–23.0
Creatinine (mg/dl)	0.7	0.72	1.03	0.03–0.50
Direct antiglobulin test	Negative	Negative	Negative	Negative
C3 (mg/dl)	28	48	33	80–165
C4 (mg/dl)	33	33	15	12–30
ADAMTS13 activity (%)	N/A	44	59	>50
Anti-FH antibody	N/A	N/A	Negative	Negative
Hematuria	3+	3+	3+	–
Proteinuria	3+	3+	3+	–
Stool culture	Negative	Negative	Negative	
Main treatment for uremia	SP inhibitor	PE, HF	PE, HF	
Outcome	Deceased	Alive (>3 years) with 2 recurrences	Alive (>6 years)	

LDH, lactate dehydrogenase; BUN, blood urea nitrogen; C3, complement component 3; C4, complement component 4; ADAMTS, a disintegrin and metalloproteinase with thrombospondi motifs; FH, factor H; N/A, not available; SP, Serine protease; PE, plasma exchange; HF, hemofiltration

Biosystems, Foster City, CA, USA). Primer sequences are available upon request. Numbering is made with the first methionine counted as 1.

SIFT and PolyPhen-2 Algorithm Analyses

We used two popular algorithms, SIFT (sift.jcvi.org) and PolyPhen-2 (genetics.bwh.harvard.edu/pph2), for predicting the damaging effects of previously identified mutations.

Structural Studies

PyMOL (www.pymol.org) was used to draw the ribbon diagram of protein structure of a single von Willebrand factor type A (VWA) domain and a carboxyl-terminal serine protease (SP) domain by using PDB file, 2WXB [11].

Results and Discussion

To demonstrate the causal factor of aHUS in this kindred, we studied complement profiles and the genomic analysis of aHUS-associated genes. We first examined the serum C3 level to screen kindred members with a predisposed aHUS condition, because a low serum C3 level that reflects complement activation and consumption is sometimes observed in aHUS patients with *CFH*, *CFI*, *CFB*, and *C3* mutations but not *MCP* mutations [4, 12]. And, we found that 9 of 12 members, including 2 affected patients (III-5 and III-6), except a deceased patient (III-2), presented low serum C3 levels in a normal situation. We also examined the well-known susceptibility genes including *CFH*, *CFI*, *CFB*, and *C3*, and identified a heterozygous *CFB* missense mutation (c.1050G>C, p.Lys350Asn) in 8 of 9 members with low C3, including 2 affected patients (III-5 and III-6), and a homozygous mutation in one unaffected member (I-2) with low C3 (Fig. 1b). No p.Lys350Asn mutations were present in an ethnically matched control population of 100 normal individuals.

So far, some researchers have reported *CFB* mutations in aHUS patients [1, 6–10]. p.Lys350Asn that we identified in this study has also been reported in sporadic case with aHUS by Roumenina et al. [7]. To review the protein function of some *CFB* mutations identified in previous reports [1, 6–10], we analyzed these reported mutations using SIFT and PolyPhen-2 algorithms. The SIFT score of p.Arg203Gln and

p.Phe286Leu was less than 0.05 (indicated to be damaging), whereas the PolyPhen-2 score of p.Arg203Gln, p.Gly254Asp, p.Phe286Leu, and p.Lys350Asn was range from 0.85 to 1.00 (indicated to be probably damaging). To further investigate how these mutations predicted to be damaging can affect the function of the protein, we next analyzed these mutations from a structural point of view. CFB is composed of an amino-terminal region of three complement control protein domains, a 40-amino acid linker region, a single VWA domain and a carboxyl-terminal SP domain [13]. When Bb fragment of CFB binds to C3b, a metal ion-dependent adhesion site is formed at the apex of the VWA domain and mediates Mg^2-dependent C3b binding [11]. Therefore, the mutation in close proximity to the Mg^2-binding site within the VWA domain, causes resistance to decay acceleration and increases C3b-binding affinity and C3bBb stability [14]. In fact, p.Phe286Leu and p.Lys350Asn in the mutations predicted to be damaging are located in close proximity to the Mg^2-binding site within the VWA domain of CFB (Fig. 1c), and these functional expression studies were reported to result in increased formation of the C3bBb complex, indicating a gain-of-function effect of CFB [6, 7]. Moreover, while we were preparing this manuscript, Roumenina and colleagues studied the functional consequences of 10 *CFB* mutations and described that 6 *CFB* mutations including p.Lys350Asn are related to aHUS pathogenesis [15]. These revealed that p.Lys350Asn is the causal factor of aHUS in this kindred from several perspectives.

In this kindred, only 3 members had aHUS, and other heterozygous mutation carriers and a homozygous mutation carrier have been in a healthy state without any diseases despite having low C3. Persistent activation of the alternative pathway by the *CFB* mutation can result in aHUS via triggering events, as reported previously [6], but the mechanism of incomplete penetrance remains unclear. Recent studies have shown that multiple disease-associated polymorphisms or at-risk CFH and MCP haplotypes are strongly associated with aHUS [6, 9, 16, 17]. To investigate the aHUS-onset-associated genetic factor, we further studied aHUS-associated genes including *MCP* and *THBD*. However, no specific mutation, polymorphism or at-risk CFH and MCP haplotypes in 2 affected members (III-5 and III-6) could be found (Supplementary Table 1 and 2). This may relate to other specific mutations, the unique nature of the affected members, or undefined aspects in the environment.

In general, the overall prognosis of patients with mutations in aHUS associated genes is poor [4, 18], but the clinical course and outcome in *CFB*-mutated aHUS patients is not well documented. In our study, although patient III-2 died of aHUS-associated myocardiopathy because of no available specific treatment at that time, patients III-5 and III-6 have had normal renal function for more than 3 and 6 years, respectively. These patients will need to be further followed up over a long period of time to study the renal outcome of aHUS patients with *CFB* mutations.

Conclusions

We described a large kindred in which a *CFB* missense mutation was the causal factor of aHUS. Phenotype-genotype correlations and outcome in *CFB*-mutated aHUS patients need to be further investigated by accumulation of a number of cases, which will lead to better treatment.

Acknowledgments We thank Masanori Matsumoto, Yoko Yoshida, and Yoshihiro Fujimura (Nara Medical University, Kashihara, Japan) for ADAMTS13 activity assay and Nobuaki Takagi and Hiromu Mae (Hyogo college of Medicine, Nishinomiya, Japan) for anti-factor H antibody assay.

This work was supported in part by Health and Labor Sciences Research Grants of Research on Measures for Intractable Diseases from the Ministry of Health, Labor and Welfare.

Declaration of Interest The authors declare that they have no conflict of interest.

References

1. Noris M, Remuzzi G. Atypical Hemolytic-Uremic Syndrome. N Engl J Med. 2009;361:1676–87.
2. Al-Herz W, Bousfiha A, Casanova JL, Chapel H, Conley ME, Cunningham-Rundles C, et al. Primary Immunodeficiency Diseases: An Update on the Classification from the International Union of Immunological Societies Expert Committee for Primary Immunodeficiency. Front Immunol. 2011;2:54.
3. Kastner DL, Aksentijevich I, Goldbach-Mansky R. Autoinflammatory Disease Reloaded: a Clinical Perspective. Cell. 2010;140:784–90.
4. Loirat C, Noris M, Fremeaux-Bacchi V. Complement and the Atypical Hemolytic Uremic Syndrome in Children. Pediatr Nephrol. 2008;23:1957–72.
5. Saunders RE, Abarrategui-Garrido C, Frémeaux-Bacchi V, de Jorge Goicoechea E, Goodship TH, López Trascasa M, et al. The Interactive Factor H-Atypical Hemolytic Uremic Syndrome Mutation Database and Website: Update and Integration of Membrane Cofactor Protein and Factor I Mutations With Structural Models. Hum Mutat. 2007;28:222–34.
6. Goicoechea de Jorge E, Harris CL, Esparza-Gordillo J, Carreras L, Arranz EA, Garrido CA, et al. Gain-of-Function Mutations in Complement Factor B are Associated With Atypical Hemolytic Uremic Syndrome. Proc Natl Acad Sci U S A. 2007;104:240–5.
7. Roumenina LT, Jablonski M, Hue C, Blouin J, Dimitrov JD, Dragon-Durey MA, et al. Hyperfunctional C3 Convertase Leads to Complement Deposition on Endothelial Cells and Contributes to Atypical Hemolytic Uremic Syndrome. Blood. 2009;114:2837–45.
8. Tawadrous H, Maga T, Sharma J, Kupferman J, Smith RJ, Schoeneman M. A Novel Mutation in the Complement Factor B Gene (CFB) and Atypical Hemolytic Uremic Syndrome. Pediatr Nephrol. 2010;25:947–51.
9. Maga TK, Nishimura CJ, Weaver AE, Frees KL, Smith RJ. Mutations in Alternative Pathway Complement Proteins in American Patients With Atypical Hemolytic Uremic Syndrome. Hum Mutat. 2010;31:E1445–60.

10. Bresin E, Rurali E, Caprioli J, Sanchez-Corral P, Fremeaux-Bacchi V, de Cordoba Rodriguez S, et al. European Working Party on Complement Genetics in Renal Diseases. Combined Complement Gene Mutations in Atypical Hemolytic Uremic Syndrome Influence Clinical Phenotype. J Am Soc Nephrol. 2013;24:475–86.
11. Forneris F, Ricklin D, Wu J, Tzekou A, Wallace RS, Lambris JD, et al. Structures of C3b in Complex With Factors B and D Give Insight into Complement Convertase Formation. Science. 2010;330: 1816–20.
12. Geerdink LM, Westra D, van Wijk JA, Dorresteijn EM, Lilien MR, Davin JC, et al. Atypical Hemolytic Uremic Syndrome in Children: Complement Mutations and Clinical Characteristics. Pediatr Nephrol. 2012;27:1283–91.
13. Mole JE, Anderson JK, Davison EA, Woods DE. Complete Primary Structure for the Zymogen of Human Complement Factor B. J Biol Chem. 1984;259:3407–12.
14. Hourcade DE, Mitchell LM, Oglesby TJ. Mutations of the Type A Domain of Complement Factor B That Promote High-Affinity C3b-Binding. J Immunol. 1999;162:2906–11.
15. Marinozzi MC, Vergoz L, Rybkine T, Ngo S, Bettoni S, Pashov A, Cayla M, Tabarin F, Jablonski M, Hue C, Smith RJ, Noris M, Halbwachs-Mecarelli L, Donadelli R, Fremeaux-Bacchi V, Roumenina LT. Complement Factor B Mutations in Atypical Hemolytic Uremic Syndrome–Disease-Relevant or Benign? J Am Soc Nephrol. 2014. doi:10.1681/ASN.2013070796.
16. Heurich M, Martínez-Barricarte R, Francis NJ, Roberts DL, de Córdoba Rodríguez S, Morgan BP, et al. Common polymorphisms in C3, factor B, and factor H collaborate to determine systemic complement activity and disease risk. Proc Natl Acad Sci U S A. 2011;108:8761–6.
17. Roumenina LT, Frimat M, Miller EC, Provot F, Dragon-Durey MA, Bordereau P, et al. A Prevalent C3 Mutation in aHUS Patients Causes a Direct C3 Convertase Gain of Function. Blood. 2012;119:4182–91.
18. Caprioli J, Noris M, Brioschi S, Pianetti G, Castelletti F, Bettinaglio P, et al. International Registry of Recurrent and Familial HUS/TTP. Genetics of HUS: The Impact of MCP, CFH, and IF Mutations on Clinical Presentation, Response to Treatment, and Outcome. Blood. 2006;108:1267–79.

VIII 先天異常/先天奇形

染色体異常・先天奇形症候群

ブルーム(Bloom)症候群

Bloom syndrome

金子英雄

Key words：小柄な体型，日光過敏性紅斑，免疫不全，高発癌，遺伝子修復異常

1. 概念・定義

Bloom症候群は免疫不全症の一つとして分類されてきた．DNAの複製・修復に関わる機構の障害は，多くの場合免疫系の障害も合併する．病因遺伝子が，すべての組織のDNAの複製・修復に関与する場合，成長障害や早老症を伴う場合が多い．DNAの複製・修復の異常が，染色体の異常を伴う場合，染色体脆弱症候群と呼ばれる．また，この場合，染色体の転座，逆位などにより発癌遺伝子の活性化もきたしやすく，遺伝性高発癌症候群と呼ばれることもある．免疫不全を伴うDNA修復異常症として，以前は，ataxia-telangiectasiaやBloom症候群などが主なものであったが，最近では，MSH6欠損症やMCM4欠損症など，新たなDNAの修復に関与する遺伝子の異常が免疫不全を呈するとして報告されている．

Bloom症候群は，生下時からの小柄な体型，日光過敏性紅斑，免疫不全症を特徴とする常染色体劣性の遺伝性疾患である[1]．なかでも，際立った特徴は，癌腫の合併が高率に認められることである．欧米での報告では，20歳代までに，約半数が何らかの癌腫を合併すると報告されている．明らかな神経症状は認められないが，軽度の学習障害が認められる場合がある．神経疾患を示す他の遺伝子修復異常症との鑑別が重要と思われる．

2. 疫　　学

厚生労働省の難治性疾患克服事業で全国の小児科，皮膚科，がん診療拠点病院に，アンケートを送り，集計したところ，9家系10症例のBloom症候群の確定例の報告があった[2]．アシュケナージジューイッシュでは保因者が約100人に1人とされている．Germanらが行っている世界のBloom症候群の登録では，134人が登録されている[3]．

3. 病　　因

病因遺伝子は，遺伝子の複製・修復に必須なRecQヘリカーゼファミリーに属するBLM遺伝子である[4]．RecQヘリカーゼファミリーには，早老症を特徴とするWerner症候群の病因遺伝子WRNや，小柄な体型，特徴的な皮疹(poikiloderma)を示すRothmund-Thomson症候群の病因遺伝子RecQL4が属している．

BLM遺伝子は15q26.1に位置し，1,417個のアミノ酸をコードしている．分子量は約160 kDaであり，中央にヘリカーゼモチーフを有し，C末にbasicなアミノ酸領域があり，核移行シグナルとして機能している[5]．我が国のBloom症候群の患者のBLM遺伝子変異を解析したところ，16 allele中9 alleleが631delCAAだった．我が国に共通な遺伝子変異と考えられた．アシュケナージジューイッシュにはBLMashと呼ばれる2281delATCTGAinsTAGATTCの共通変異

Hideo Kankeo: Department of Clinical Research, National Hospital Organization, Nagara Medical Center　国立病院機構長良医療センター　臨床研究部

0047-1852/14/¥60/頁/JCOPY

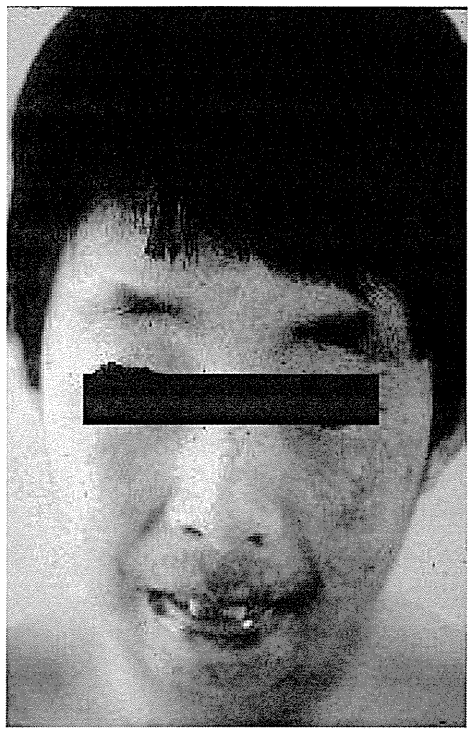

図1 Bloom症候群の日光過敏性紅斑

が認められる．BLMタンパクは姉妹相同組換えの抑制に必須のタンパクである．また，BLMの障害されている細胞では姉妹相同組換え以外のほかの染色体異常も生じやすい．BLMタンパクは他の複製・修復に関わるタンパクと複合体を形成して機能している[6]．

4. 病　　態

日光過敏性紅斑(多くは頬部に対称的)は特徴的であるが加齢に伴い消失することもある(**図1**)．生下時から均整のとれた小柄な体型が認められる．多くの症例は，生下時の体重が2,500g未満の低出生体重児である．免疫不全症も特徴とされているが，我が国での集計では，易感染の程度はそれほど強くなかった．骨髄異形成症候群が2例に認められていた．また，鳥様顔貌といわれる特徴的な顔貌が認められることもある．糖尿病は10例中5例に認められ，特徴的な合併症である．I型，II型の糖尿病とも認められた．性腺機能低下(早期の閉経，不妊)，若年性白内障，慢性肺疾患も本症を疑わせる所見となる．

癌腫の種類は欧米での報告では，基礎疾患を有しない各年齢に発症する癌腫の発症がすべて高率になるとされている．すなわち，若年では，白血病・リンパ腫などの肉腫が高率に認められ，成人以降は，大腸癌，肺癌といった上皮系の腫瘍が高率に発症するとされている．我が国の集計では，10例中6例にB細胞系のリンパ腫が認められた．

検査所見として血清IgM 50mg/dL以下の低値が半数以上に認められ，Bloom症候群の免疫不全の特徴と考えられた．Bloom症候群を疑った場合は，姉妹染色分体組換えの頻度の検査を行う．組換えの頻度は，Bloom症候群では，健常人と比較して数十倍に増加している．

5. 診断と鑑別診断

姉妹染色分体組換えの頻度の上昇が認められた場合は，暫定的にBloom症候群とする．最終的には，BLM遺伝子の検索を行い確定診断とする．鑑別として，RecQヘリカーゼ遺伝子異常により発症するRothmund-Thomson症候群，Werner症候群などを鑑別する．Cockayne症候群，Fanconi症候群，毛細血管拡張性失調症，色素性乾皮症，先天性角化症などの遺伝子の複製・修復に関与する遺伝子の障害による疾患が，一部同様な表現型を有することから鑑別に挙がる．しかし，姉妹染色分体組換えの頻度の上昇は，Bloom症候群に特徴的である．臨床症状，IgMの低下に加えて姉妹染色分体組換えの頻度の上昇を認めた場合，BLM遺伝子の解析を行い，確定診断を行う(**図2**)．

6. 治療と予後

対症療法が基本となる．発癌に対して早期に発見し，早期に治療することが基本方針である．血液検査，各種の画像検査を定期的に行う．放射線感受性がataxia-telangiectasiaほどではないが認められるとの報告もあり，放射線を用いる検査は必要最低限とし，エコー，MRIなどを用いる．発癌した場合の治療法としては，どのようなプロトコールを用いるかに関して，明ら

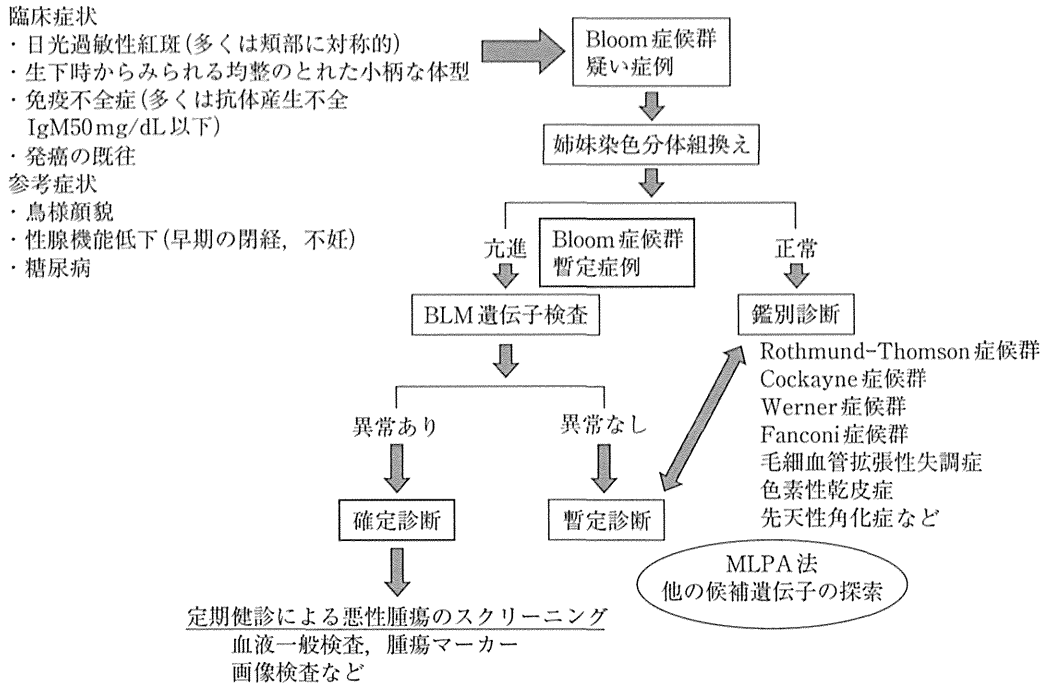

図2　Bloom症候群診断指針

かなエビデンスはない．多くはその症例ごとに対応されている．抗癌剤に対する感受性が亢進していると考えられるため，著者らの症例も含めて通常のプロトコールの半量程度で行われることが多い[7]．今後，症例を集積しての検討が必要と考えられる．発癌に対して早期から対処することで，QOLの向上，予後の改善につなげることができると考えられる．

文　献

1) Bloom D: Congenital telangiectatic erythema resembling lupus erythematosus in dwarfs. Am J Dis Child **88**: 754-758, 1954.
2) 金子英雄(研究代表者): 遺伝子修復異常症(Bloom症候群，Rothmund-Thomson症候群，RAPADILINO症候群，Baller-Gerold症候群)の実態調査，早期診断法の確立に関する研究．厚生労働省科学研究費補助金難治性疾患克服研究事業．平成23年度 総括・分担研究報告書．
3) German J, et al: Syndrome-causing mutations of the BLM gene in persons in the Bloom's syndrome registry. Hum Mutat **28**: 743-753, 2007.
4) Ellis NA, et al: The Bloom syndrome gene product is homologous to RecQ helicases. Cell **83**: 655-666, 1995.
5) Kaneko H, et al: BLM(the causative gene of Bloom syndrome) protein translocation into the nucleus by a nuclear localization signal. Biochem Biophys Res Commun **240**: 348-353, 1997.
6) Wang Y, et al: BASC, a super complex of BRACA1-associated proteins involved in the recognition and repair of aberrant DNA structures. Genes Dev **14**: 927-939, 2000.
7) Kaneko H, Kondo N: Clinical features of Bloom syndrome and function of the causative gene, BLM helicase. Expert Rev Mol Diagn **4**: 393-401, 2004.

VIII 先天異常/先天奇形

染色体異常・先天奇形症候群

Baller-Gerold 症候群

Baller-Gerold syndrome

金子英雄

Key words：頭蓋縫合早期癒合症，橈骨欠損，小柄な体型，RecQL4

1. 概　　念

Baller-Gerold 症候群は冠状縫合の早期癒合による狭頭症と橈骨欠損・低形成を特徴とするまれな常染色体劣性の遺伝性疾患である．冠状縫合の早期癒合のため，短頭型頭蓋，眼球突出，前頭部の突出を伴い特徴的な顔貌を呈する[1]．母指欠損，多形皮膚萎縮症も本症候群の特徴である．Baller と Gerold が独立して，狭頭症に橈骨欠損を伴う患者を報告したのが始まりである．病因遺伝子は，遺伝子の複製・修復に必須な RecQ ヘリカーゼファミリーに属する RecQL4 遺伝子である[2]．本症候群は同じ RecQL4 遺伝子の異常により発症する Rothmund-Thomson 症候群，RAPADILINO 症候群や他の遺伝子修復異常症との異同が問題となる[2]．

2. 疫　　学

厚生労働省の難治性疾患克服事業で，全国の小児科，皮膚科，がん診療拠点病院に，アンケートを送り，集計したところ，一次アンケートで報告があった施設は，RAPADILINO 症候群 3 施設，Baller-Gerold 症候群 1 施設であった[3]．この施設に二次調査票を送り，最終的に RAPADILINO 症候群 1 例，Baller-Gerold 症候群 2 例(兄弟例)が確認されている．我が国では非常にまれな疾患と考えられるが，見逃されている症例も存在すると思われる．

3. 病　　因

RecQ ヘリカーゼファミリーに属する RecQL4 遺伝子の障害により発症する[4]．DNA の複製の開始に関与し，様々な遺伝子修復の過程にも関与している．RecQ ヘリカーゼファミリーには，早老症を特徴とする Werner 症候群の病因遺伝子 WRN や，小柄な体型，日光過敏性紅斑，免疫不全，高発癌を特徴とする Bloom 症候群の病因遺伝子 BLM が属している．RecQL4 は ATP 依存性の DNA ヘリカーゼモチーフの構造をコードしている．1,208 個のアミノ酸より構成されている．ヘリカーゼは二本鎖 DNA の水素結合を分解し一本鎖に巻き戻す作用を有する．RecQL4 の機能低下により，DNA の複製・修復の障害が生じ様々な症状が出現すると考えられる．一方，頭蓋骨早期癒合と上肢の奇形から Baller-Gerold 症候群と診断されていた症例に Saethre-Chotzen 症候群の病因遺伝子である TWIST 遺伝子異常が同定された報告もある[5,6]．

4. 病　　態

頭蓋骨早期癒合，橈骨欠損・低形成が特徴である(**図 1**)．頭蓋は短く，相対的に三角頭蓋を示すこともある．冠状縫合の早期癒合による短頭，前頭の突出，眼球の突出，耳介低位，橈骨欠損，拇指の欠損，尺骨の短縮などが認められる．これらは，非対称的に認められることもある．膝蓋骨の無・低形成が認められる．肛門が

Hideo Kankeo: Department of Clinical Research, National Hospital Organization, Nagara Medical Center 国立病院機構長良医療センター 臨床研究部

0047-1852/14/¥60/頁/JCOPY

図1 Baller-Gerold症候群の顔貌と皮膚所見

[Reprinted from Van Maldergem L, et al: Revisiting the craniosynostosis-radial ray hypoplasia association: Baller-Gerold syndrome caused by mutations in the RECQL4 gene. J Med Genet 43: 148-152, 2006, Copyright © 2006 Lionel Van Maldergem. All right reserved.]

前方に位置している症例も報告されている．乳児期早期には皮膚所見は認められないが，次第に皮膚所見が著明となる．まず上肢，下肢に多形皮膚萎縮症が認められるようになる．水疱が顔から臀部，四肢へと広がる．数年後には色素が消失し，萎縮，毛細血管拡張が認められる．小児期は成長障害が著明である．身長，体重は平均の4SD以下のことが多い．膝蓋骨の欠損のため，膝部はそりかえり動揺が認められる．10代から20代に骨肉腫，白血病・リンパ腫，皮膚癌などの合併が報告されている．

5. 診断と鑑別診断

診断は冠状縫合の早期癒合，橈骨欠損，発達遅滞，多形皮膚萎縮症がそろった場合疑い症例とする．冠状縫合の早期癒合は3D-CT画像が有用である．橈骨欠損は，手指欠損または母指欠損を伴うことが多い．

橈骨欠損と頭蓋骨早期癒合の合併が認められた場合，ファンコニー貧血(OMIM #227650)，Roberts症候群(OMIM #268300)，橈骨欠損を伴う血小板減少症(OMIM #274000)，Holt-Oram症候群(OMIM #142900)，SALL4関連症候群，Saethre-Chotzen症候群(OMIM #101400)，VACTER症候群，胎児バルプロ酸症候群などが鑑別に挙がる．本症候群が臨床上疑われた場合，最終的には遺伝子解析を行う．同じRecQL4遺伝子異常により，Rothmund-Thomson症候群，RAPADILINO症候群が発症する(図2)．Rothmund-Thomson症候群は，顔の多形皮膚萎縮症，低身長，骨格異常(橈骨欠損，鞍鼻)，日光過敏症，毛髪異常(疎な毛髪)，無または疎な睫毛，若年性白内障，早老症，高発癌(骨肉腫)を特徴とする．RAPADILINO症候群は，以下の特徴の頭文字から取った疾患名である．橈骨欠損・低形成(radial hypoplasia/aplasia)，膝蓋骨低形成(patella hypoplasia)，口蓋の低形成，口蓋裂(cleft palate)，慢性の下痢(diarrhea)，関節の脱臼(dislocated joints)，小柄な体型(little size)，四肢の奇形(limb malformation)，細長い鼻(nose slender)，正常な知能(normal intelligence)，多形皮膚萎縮は認められない．同じRecQL4の異常であっても，表現型が異なるのはRecQL4が複雑で多様な細胞内のネットワークに関与していると考えられている[7]．一方，Baller-Gerold症候群，Rothmund-Thomson症候群，RAPADILINO症候群は，臨床上もオーバーラップしており，これらの症候群まと

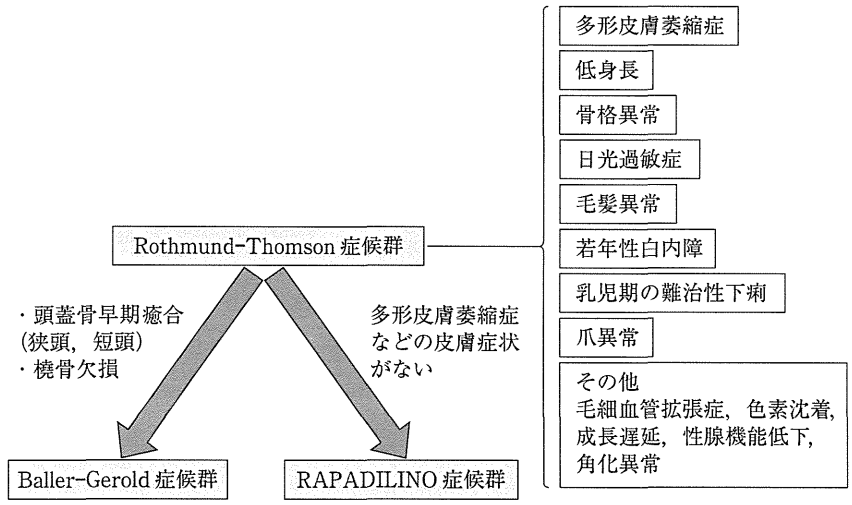

図2　Rothmund-Thomson，RAPADILINO，Baller-Gerold 症候群診断指針
これらの3つの症候群は，RecQL4の障害により発症する一群と，別の病因により発症するものも含まれている．RecQL4遺伝子異常を示す疾患群を区別せずに一個の疾患単位としてとらえる方がわかりやすいとも考えられる．

めて，RecQL4異常症として一つの疾患概念とした方がよいとの報告もある[4,8]．

6. 治療と予後

両側の頭蓋縫合早期癒合症の場合は生後6カ月までに手術を行うとの報告がある．母指欠損に対して，母指形成術が行われる．発達などのチェックも必要である．定期的な検診により癌腫(特に骨肉腫)の発生を早期に発見し，外科的切除，抗癌剤による治療を行う．

発癌した場合の治療法としてどのようなプロトコールを用いるかに関して，明らかなエビデンスはない．多くはその症例ごとに対応されている．抗癌剤に対する感受性が亢進していると考えられるため，プロトコールの変更が必要な場合もある．今後，症例を集積しての検討が必要と考えられる．発癌に対して早期から対処することで，QOLの向上，予後の改善につなげることができると考えられる．

文　献

1) Van Maldergem L: Baller-Gerold Syndrome. 2007. In: GeneReviews™(ed by Pagon RA, et al), [Internet]. University of Washington, Seattle, Seattle(WA), 1993-2013.
2) Larizza L, et al: Rothmund-Thomson syndrome. Orphanet J Rare Dis **29**(5): 2, 2010.
3) 金子英雄(研究代表者): 遺伝子修復異常症(Bloom症候群，Rothmund-Thomson症候群，RAPADILINO症候群，Baller-Gerold症候群)の実態調査，早期診断法の確立に関する研究．厚生労働省科学研究費補助金難治性疾患克服研究事業．平成24年度総括・分担研究報告書．
4) Van Maldergem L, et al: Revisiting the craniosynostosis-radial ray hypoplasia association: Baller-Gerold syndrome caused by mutations in the RECQL4 gene. J Med Genet **43**(2): 148-152, 2006.
5) Gripp KW1, et al: TWIST gene mutation in a patient with radial aplasia and craniosynostosis: further evidence for heterogeneity of Baller-Gerold syndrome. Am J Med Genet **82**(2): 170-176, 1999.
6) Seto ML1, et al: Another TWIST on Baller-Gerold syndrome. Am J Med Genet **104**(4): 323-330, 2001.
7) Kellermayer R: The versatile RECQL4. Genet Med **8**(4): 213-216, 2006.
8) Mégarbané A, et al: Overlap between Baller-Gerold and Rothmund-Thomson syndrome. Clin Dysmorphol **9**(4): 303-305, 2000.

nature COMMUNICATIONS

ARTICLE

Received 26 Aug 2014 | Accepted 19 Nov 2014 | Published 14 Jan 2015

DOI: 10.1038/ncomms6931

FBH1 influences DNA replication fork stability and homologous recombination through ubiquitylation of RAD51

Wai Kit Chu[1,2,*], Miranda J. Payne[1,*], Petra Beli[3], Katsuhiro Hanada[1], Chunaram Choudhary[3] & Ian D. Hickson[1,2]

Unscheduled homologous recombination (HR) can lead to genomic instability, which greatly increases the threat of neoplastic transformation in humans. The F-box DNA helicase 1 (FBH1) is a 3′–5′ DNA helicase with a putative function as a negative regulator of HR. It is the only known DNA helicase to contain an F-box, suggesting that one of its functions is to act as a ubiquitin ligase as part of an SCF (SKP1, CUL1 and F-box) complex. Here we report that the central player in HR, RAD51, is ubiquitylated by the SCF^{FBH1} complex. Expression of an ubiquitylation-resistant form of RAD51 in human cells leads to hyperrecombination, as well as several phenotypes indicative of an altered response to DNA replication stress. These effects are likely to be mediated by the enhanced nuclear matrix association of the ubiquitylation-resistant RAD51. These data are consistent with FBH1 acting as a negative regulator of RAD51 function in human cells.

[1] Weatherall Institute of Molecular Medicine, University of Oxford, John Radcliffe Hospital, Oxford OX3 9DS, UK. [2] Center for Healthy Aging, Department of Cellular and Molecular Medicine, Panum Institute, University of Copenhagen, Blegdamsvej 3B, 2200 Copenhagen N, Denmark. [3] Novo Nordisk Foundation Center for Protein Research, University of Copenhagen, 2200 Copenhagen N, Denmark. * These authors contributed equally to this work. Correspondence and requests for materials should be addressed to I.D.H. (email: iandh@sund.ku.dk).

Faithful DNA replication is essential for cell proliferation. Nevertheless, a number of circumstances can arise in cells that lead to the stalling or collapse of DNA replication forks. On short-term replication blockage, such as following exposure of cells to the ribonucleotide reductase inhibitor, hydroxyurea (HU), the replication machinery is stalled, but remains bound to the DNA[1]. If the duration of replication stalling is prolonged, the replisome components can detach from the stalled fork, and the exposed fork can be processed into a double-strand break (DSB). This fork breakage process is most probably mediated by the DNA structure-specific endonuclease MUS81-EME1 (ref. 2). Under these circumstances, the fork is deemed to have 'collapsed'. Stalled and collapsed forks both require the protective function of the RAD51 recombinase, but different roles of RAD51 are apparently required in each case. In the case of a stalled fork, RAD51 serves to stabilize the fork, in a process that does not appear to require the canonical homologous recombination (HR) machinery. In this pathway, RAD51 has been proposed to coat the single-stranded DNA (ssDNA) region adjacent to the stalled fork, potentially facilitating the formation of a Holliday junction via so-called fork regression (reversal), which involves the annealing of the two nascent DNA strands[3]. Indeed, the RAD51 homologue in *Escherichia coli*, RecA, has been demonstrated to promote this process *in vitro*[4]. In addition, RAD51 has been reported to protect the nascent DNA from MRE11-mediated degradation at stalled replication forks[5,6]. In contrast to this HR-independent function of RAD51, the canonical HR pathway is known to operate at collapsed forks, where a DSB is generated. One of the key steps in repair of the single-ended DSB formed at a collapsed fork is the formation of a RAD51 protein filament on the ssDNA generated by DSB end resection. This nucleoprotein filament is required for the search for a homologous DNA sequence and for repair of the break[7]. RAD51 is also involved in the reassembly of key DNA replication proteins, including the so-called CMG complex comprising CDC45-MCM-GINS, after replication forks have collapsed[8]. Despite this protective role of RAD51 and HR factors more generally at stalled/collapsed replication forks, it is clear that uncontrolled HR can lead to genome rearrangements and loss of heterozygosity, which are potent drivers of tumorigenesis[9]. As RAD51 is a key player in replication-associated HR, controlling the binding of RAD51 to its potential DNA substrates or to chromatin more generally would be an effective means to regulate the balance between the beneficial and detrimental roles of HR in an effort to preserve genome stability.

Several DNA helicases have been identified that can control the stability of a RAD51 nucleoprotein filament[10–13]. Many of these belong to the UvrD family of proteins, such as Srs2 in yeast and PARI in mammals[12–14]. Mammalian cells express another UvrD family member, FBH1 (F-box DNA helicase 1), which has been reported previously to suppress HR[15]. FBH1 is conserved in human, mouse and *Schizosaccharomyces pombe* cells, but is not found in *Saccharomyces cerevisiae*[16]. In addition to the helicase domain, there is an amino-terminal F-box domain present in FBH1. F-box proteins form part of the so-called SCF complexes (SKP1-CUL1-F-box protein), which generally act as E3 ubiquitin ligases[17]. Ubiquitylation is a posttranslational modification that leads to the covalent attachment of the ubiquitin peptide to particular lysine residues in the target protein. This modification may regulate the substrate's function or target the substrate for proteasomal degradation[17]. Previous data derived from studies in *S. pombe* have suggested that both the F-box domain and the helicase domain of Fbh1 are required for the repair of DNA damage in that organism, although the helicase function seems more critical[18,19]. Moreover, genetic analysis suggested that yeast Fbh1 acts downstream of Rad51 in the HR pathway[18,20]. Consistent with this, the level of Rad51 nuclear foci is greatly increased in Fbh1-deficient yeast, a phenotype that is also characteristic of FBH1-depleted human cells[15,21,22]. Recently, we found that the helicase function of FBH1 co-operates with the MUS81-EME1 nuclease in generating DSBs following replication stress induced by HU[23]. FBH1 is often mutated in melanoma cells, which suggests that the DSBs generated in this context by the action of FBH1 might serve to trigger apoptosis, to prevent oncogenic transformation[24,25]. Interestingly, human and mouse cells expressing a helicase-dead version of FBH1 are resistant to the cytotoxic effects of replication stress induced by HU[23]. In addition, FBH1 forms HU-induced nuclear foci that co-localize with the ssDNA-binding protein, RPA[15]. These observations strongly implicate the helicase function of FBH1 in coping with some aspect of DNA replication stress. Consistent with this, recent data indicate that human FBH1 can displace RAD51 filaments from ssDNA[22]. However, the role of the F-box domain of FBH1 remains undefined.

Although UvrD family helicases are implicated in the regulation of RAD51 function in a diverse range of cell types, it is not clear whether the F-box also plays a role in regulating RAD51 or HR more generally in mammalian cells. Indeed, it has been reported that an F-box-mutated variant of *S. pombe* Fbh1 is largely functional, which implies the F-box may only play a minor role in HR and in the cellular response to replication problems in that organism[18]. In human cells, the substrate of the FBH1 ubiquitylation and the role of the F-box in pathways for coping with replication stress are currently unknown. Here we have addressed these issues. We demonstrate that RAD51 can be ubiquitylated by the SCF^{FBH1} complex *in vitro*. In cells expressing an ubiquitylation-resistant form of RAD51, the RAD51 protein shows enhanced chromatin association during replication stress. In these cells, the frequency of replication fork stalling is reduced, while recovery of replication following replication stress is enhanced. These cells also show increased resistance to replication inhibitors, and hyperrecombination, consistent with a role for FBH1 in regulating RAD51 function in human cells.

Results

RAD51 is ubiquitylated by the SCF^{FBH1} complex *in vitro*. The FBH1 protein is implicated in the control of RAD51 function, most probably in the context of stalled or damaged DNA replication forks. Although the helicase function of FBH1 is thought to regulate the stable association of RAD51 with DNA, the role of the F-box domain in FBH1 has not been defined. To investigate the function of the F-box, we purified recombinant human FBH1, together with the other SCF complex components, as well as human RAD51 protein (Supplementary Fig. 1a,b). The purified SCF^{FBH1} complex was then tested for its ability to ubiquitylate the purified RAD51 protein *in vitro*. In the presence of SCF^{FBH1} and ubiquitin, a new species of the RAD51 protein (which normally migrates at 37 kDa on SDS–polyacrylamide gel electrophoresis (PAGE)) was observed with a migration equivalent to 50 kDa (Fig. 1a). This would be consistent with the addition of a single ubiquitin moiety to the RAD51 protein. To confirm that this protein modification was via ubiquitylation, we repeated the reactions using haemagglutinin (HA) epitope-tagged ubiquitin instead of untagged ubiquitin. In this case, the modified RAD51 showed a further reduction in mobility on SDS–PAGE due to the presence of the HA tag (Fig. 1a). Hence, we conclude that SCF^{FBH1} can ubiquitylate RAD51 *in vitro*. This modification required, as expected, an E1 enzyme and an E2 enzyme (Supplementary Fig. 1c), but occurred independently of the presence or absence of ssDNA (Fig. 1b). A negative control reaction is shown in Fig. 1d described below, to demonstrate a

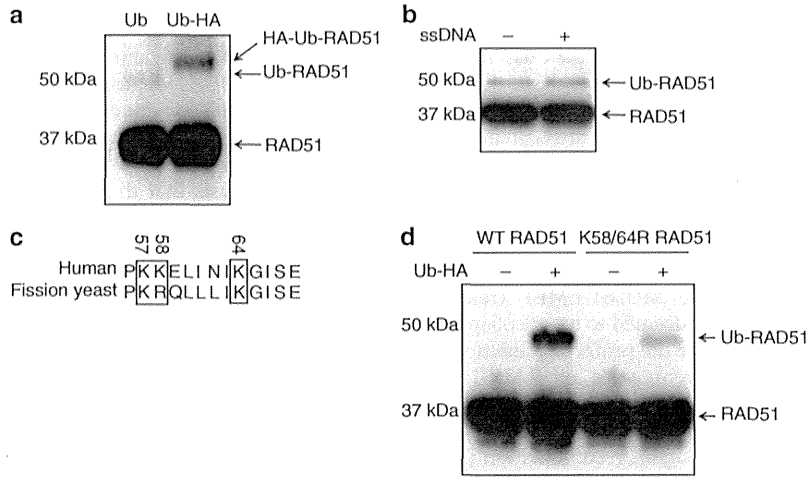

Figure 1 | RAD51 is ubiquitylated *in vitro* by FBH1. (**a**) Western blotting of products from ubiquitylation of RAD51 by SCF^{FBH1} probed with an anti-RAD51 antibody. The positions of the unmodified RAD51, the ubiquitylated RAD51 (ub-RAD51) and the HA-Ub RAD51 are shown on the right. (**b**) The ubiquitylation of RAD51 by SCF^{FBH1} has no requirement for ssDNA. (**c**) Protein sequence alignment of a region of the human and *S. pombe* RAD51 proteins. The conserved lysines/arginines are bracketed and their positions are numbered above. (**d**) WT RAD51 or RAD51 containing mutations of lysines to arginines on position 58 and 64 (K58/64R) were subjected to *in vitro* ubiquitylation by SCF^{FBH1}. The + and − symbols denote the presence or absence of the indicated protein, respectively. A western blot is shown of the products of the assay probed with an anti-RAD51 antibody.

requirement for ubiquitin itself. The preferred E2 appeared to be UbcH5a, which could not be replaced by Cdc34 or UbcH6 (Supplementary Fig. 1c,d). The reaction was also not stimulated by the presence of Nedd8 (Supplementary Fig. 1c). To assess whether there was any specificity to the reaction, we replaced RAD51 with RPA, FANCD2 or BLM protein. In none of these cases could we detect ubiquitylation by the SCF^{FBH1} complex (Supplementary Fig. 1e).

Identification of the sites of ubiquitylation on RAD51. A previous proteome-wide mass spectrometry study identified K58 and K64 on RAD51 as being ubiquitylated in human cells[26]. To identify whether these lysine residues could be targeted by SCF^{FBH1}, we subjected the *in vitro* ubiquitylated RAD51 to mass spectrometry following trypsin digestion. This analysis provided 79% sequence coverage of RAD51. Five modified residues were identified within the population of RAD51 protein molecules, of which the most prominent were K58 and K64 (Supplementary Table 1). K58 and K64 are in the N-terminal domain of RAD51, which lies outside of the core 'RecA-like' ATPase domain. Nevertheless, the region of RAD51 around K58/64 is conserved (Fig. 1c), despite the lack of overall conservation of the N-terminal domains of eukaryotic RAD51 proteins. To investigate the importance of the K58/64 residues in the modification of RAD51 by SCF^{FBH1}, we purified a version of RAD51 containing arginine substitutions of K58 and K64. This protein, designated K58/64R RAD51, possessed a similar ability to interact physically with GST-FBH1 as did the WT RAD51 (Supplementary Fig. 1f). However, K58/64R RAD51 was ubiquitylated much less efficiently by FBH1 *in vitro* than was wild-type (WT) RAD51 (Fig. 1d), confirming that the primary sites of modification by FBH1 on RAD51 are K58 and K64.

Role of RAD51 ubiquitylation in human cells. Next, we investigate the role of K58/64 modification of RAD51 in human cells. To do this, we compared the phenotype of U2OS cells expressing either WT RAD51 or K58/64R RAD51. We reasoned that a ubiquitylation-resistant form of RAD51 might potentially escape the control imposed by FBH1, and therefore be dominantly acting even in cells expressing endogenous RAD51. We focused on the cellular response to replication stress, because our previous studies indicated that FBH1-deficient mouse embryonic stem (ES) cells are abnormally resistant to HU-induced replication fork perturbation[23]. This resistance is manifested both as an increase in clonogenic survival after HU treatment and a decrease in DSB induction compared with WT cells. To analyse the effects of K58/64 ubiquitylation, we generated stable transfectants of U2OS cells expressing either WT or K58/64R RAD51. The level of transfected RAD51 was equal in both cases, and was in excess over that of the endogenous RAD51 by approximately twofold (Fig. 2a). Despite lacking any additional tag (because tags are known to adversely affect RAD51 function), the transfected RAD51 had a slightly slower mobility on SDS–PAGE compared with the endogenous protein. This phenomenon has been observed in a previous study[27]. Confirmation that the protein species recognized by this antibody were all RAD51 came from analysis and cells exposed to a small interfering RNA (siRNA) targeted to the coding region of RAD51. After transfection of this siRNA, the level of the endogenous and transfected RAD51 was diminished greatly (Fig. 2a).

Next, we investigated the phenotypic affects of the transfected K58/64R RAD51. Consistent with previous data indicating that *FBH1* gene mutation confers resistance to HU, we found that the cells expressing K58/64R RAD51 were significantly more HU resistant than the isogenic control cells expressing WT-transfected RAD51 (Fig. 2b; $P<0.05$ using an unpaired *t*-test). In cells expressing K58/64R RAD51, the HU resistance was also significant when the endogenous RAD51 protein was depleted using an siRNA targeting the 3′-untranslated region (3′-UTR) of *RAD51*, a region of the *RAD51* gene that is absent from the transfected *RAD51* complementary DNAs (Supplementary Fig. 2a,b). These data argue that the endogenous RAD51 does not interfere with the 'dominant' phenotypic effects seen when expressing ubiquitylation-resistant RAD51. Moreover, pulsed-field gel electrophoresis analysis indicated that the K58/64R RAD51-expressing cells accumulated significantly fewer DNA DSBs than did the WT RAD51-expressing cells following a 24-h exposure to HU (Fig. 2c; $P<0.05$ using an unpaired *t*-test). In cells expressing K58/64R RAD51, there was also a diminution in

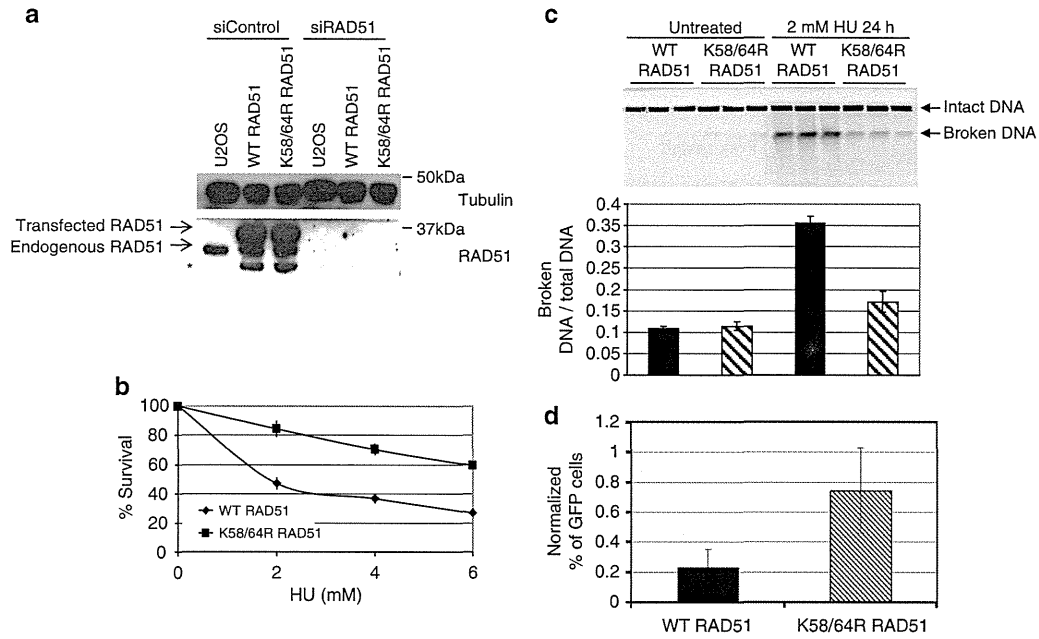

Figure 2 | Expression of K58/64R RAD51 influences the cellular response to HU. (**a**) Western blotting of cells transfected with empty vector or a construct expressing either WT RAD51 or K58/64R RAD51, as indicated above the lanes. The set of three samples on the right were derived from cells treated with an siRNA targeted against the coding region of *RAD51*, to demonstrate the specificity of the antibody. The positions of the transfected and endogenous RAD51 species are indicated on the left. Tubulin was used as a loading control. The asterisk marks degradation products of RAD51, which were reported previously[48]. (**b**) Clonogenic survival curves following exposure of WT RAD51- and K58/64R RAD51-expressing cells to HU, as indicated in the key. Points represent the mean of three independent determinations. (**c**) Induction of DSBs by treating cells with 2 mM HU for 24 h. The upper panel shows a representative pulsed field gel with triplicate samples for each, while the lower panel shows data for the average of three independent experiments. Bands were quantified by using ImageJ software. (**d**) Hyperrecombination in K58/64R RAD51-expressing cells as determined by using the DR-GFP assay. The percentage of cells expressing GFP was normalized to a control (a plasmid expressing RFP under the control of the same promoter). The means for two independent experiments are shown. Error bars represent s.d.

the level of DNA DSBs following HU treatment when the endogenous RAD51 was depleted by an siRNA targeting the 3′-UTR of *RAD51* (Supplementary Fig. 2c). This difference in DSB levels required that the cells be subjected to prolonged HU treatment, and was much less evident after only a 12-h exposure to HU (Supplementary Fig. 2d). Interestingly, we found that the resistance to replication stress in K58/64R RAD51-expressing cells was not limited to HU, but was also seen with aphidicolin, which acts via a different mechanism from HU (direct polymerase inhibition, not dNTP depletion) (Supplementary Fig. 2e). However, the K58/64R RAD51-expressing cells were not hyperresistant to ionizing radiation (Supplementary Fig. 2f), suggesting a role for RAD51 ubiquitylation only during the cellular response to DNA replication stress.

Loss of FBH1 helicase function in mouse ES cells leads to spontaneous hyperrecombination, presumably because RAD51 escapes the normal control imposed by FBH1 (ref. 22). Using the widely used and previously validated direct repeat-green fluorescent protein (DR-GFP) assay[28], we found that the U2OS cells expressing K58/64R RAD51 also showed an approximately threefold increase in the level of recombination compared with control cells expressing WT RAD51 only (Fig. 2d; $P<0.05$ using an unpaired *t*-test). In cells expressing K58/64R RAD51, the level of recombination was also significantly higher when the endogenous RAD51 was depleted by an siRNA targeting the 3′-UTR of *RAD51* (approximately fourfold; Supplementary Fig. 2g,h).

Next, we investigated whether cells expressing either WT or K58/64R RAD51 responded differently following release from prolonged HU-induced arrest. To do this, the DNA fibre technique was employed to quantify replication dynamics. Active replicons were initially labelled by incorporation of CldU and then replication was arrested by exposure of cells to HU. Following removal of the HU, the ability of the cells to recover productive DNA replication was monitored by incorporation of IdU. Three categories of replication were quantified, as depicted in Fig. 3a: (i) irreversibly stalled forks (CldU tracts only; marked in red); (ii) forks that were competent to restart after HU exposure (adjacent red and green (IdU) tracts); (iii) new origin firing (IdU/green tracts only). In the absence of HU, there was no statistically significant difference between any of these replication parameters in cells expressing WT RAD51 or K58/64R RAD51 protein (Fig. 3b). In contrast, following a 24-h exposure to HU, there was a significant change in the proportion of forks that remained stalled or were able to restart. For the K58/64R RAD51-expressing cells, a smaller proportion of replication forks were irreversibly stalled and a correspondingly greater proportion of forks successfully re-initiated DNA synthesis compared with cells expressing WT RAD51 (Fig. 3b). Although new origin firing also appeared suppressed in the K58/64R RAD51 cells compared with the control cells, this difference did not reach statistical significance. Equivalent results were also observed in K58/64 RAD51-expressing cells in which the endogenous RAD51 was depleted using an siRNA targeting the 3′-UTR of RAD51 (Supplementary Fig. 3).

RAD51 ubiquitylation controls subcellular localization. It has been reported that both mouse ES cells lacking FBH1 helicase function and FBH1-depleted human cells show increased levels of RAD51 nuclear foci[15]. We analysed, therefore, whether

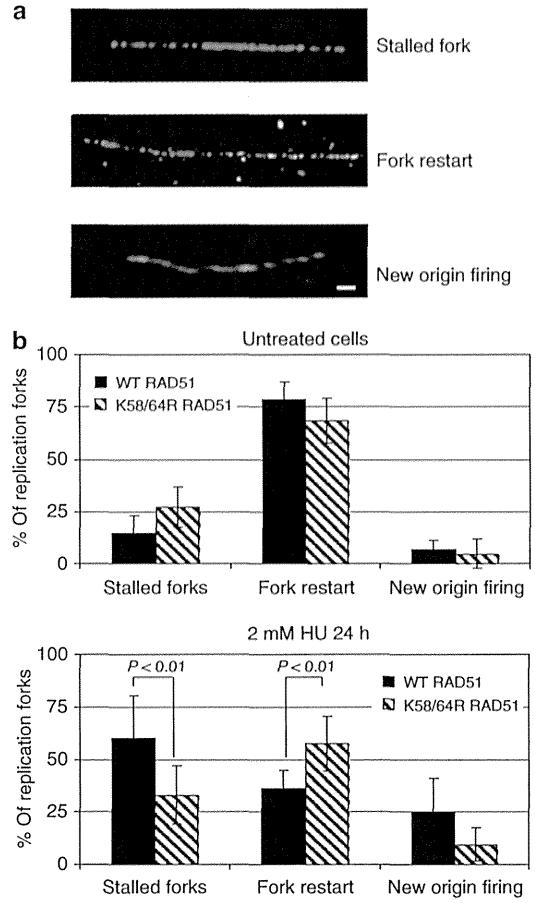

Figure 3 | Ubiquitylation on RAD51 influences replication fork restart. (**a**) Representative pictures of a stalled fork, fork restart and new origin firing from cells exposed to 2 mM HU for 24 h. DNA synthesis occurring before or after HU treatment was stained as red and green tracts, respectively. Scale bar, 1 μm (white). (**b**) Quantification of the percentage of replicons with stalled forks, re-started forks or newly fired origins for cells expressing WT RAD51 (black bars) or K58/64R RAD51 (hatched bars). The upper panel shows untreated cells and the lower panel shows cells exposed to HU for 24 h. The means are shown for two independent experiments. Where significant ($P<0.01$), *P*-values are indicated. At least 180 forks for each cell line were quantified and the differences in the distributions of stalled forks and fork restart after HU treatment were evaluated statistically using an unpaired *t*-test. Error bars represent s.d.

ubiquitylation of RAD51 was important for regulating the subcellular localization of RAD51. For this, we treated cells with 2 mM HU for 24 h, as we had seen the most dramatic differences in the levels of DSBs using this regimen. Using fluorescence microscopy, we found a reduced level of the ubiquitylation-resistant RAD51 localized to the cytoplasm, as compared with cells expressing the WT RAD51 protein (Fig. 4a,b; $P<0.05$ using an unpaired *t*-test). Consistent with this, a correspondingly increased number of RAD51 nuclear foci were evident in the K58/K64 RAD51-expressing cells (Fig. 4c; $P<0.05$ using an unpaired *t*-test, compared with the WT RAD51 cells). Importantly, these experiments were performed without permeabilizing the cell membrane before fixing the cells, to preserve the cytoplasmic RAD51 signal. Following depletion of the endogenous RAD51 messenger RNA, the cells were also analysed for the subcellular localization of the transfected RAD51. As shown in Supplementary Fig. 4a, there was a substantial difference in the percentage of cells expressing RAD51 in the cytoplasm, with an approximately tenfold greater proportion of cytoplasmic RAD51 seen in the cells expressing WT RAD51 compared with those expressing K58/64R RAD51, confirming the data presented in Fig. 4a–c. Consistent with these immunofluorescence data, we demonstrated that the K58/64R RAD51 was approximately equally distributed between the chromatin and soluble fractions, whereas the WT RAD51 was strongly concentrated in the soluble fraction (Fig. 4d). This localization bias was not affected by depleting the endogenous RAD51 with an siRNA targeting the 3′-UTR of *RAD51* (Supplementary Fig. 4b).

RAD51 ubiquitylation does not prevent BRCA2 interaction. The BRCA2 protein has been shown to interact with and stimulate RAD51 loading onto RPA-coated ssDNA[29–32]. Therefore, we tested the proposal that RAD51 ubiquitylation might interfere with its ability to interact with BRCA2. To do this, we analysed the co-immunoprecipitation of RAD51 or K58/64 RAD51 with BRCA2 in cells in which the endogenous RAD51 had been depleted. As shown in Fig. 5, the WT and K58/64R RAD51 proteins were equally effective at co-immunoprecipitating endogenous BRCA2, suggesting that ubiquitylation of RAD51 does not affect the RAD51–BRCA2 interaction.

Discussion

The UvrD family of DNA helicases appears to play a number of roles in the cellular response to both DNA damage and DNA replication stress. Some, but not all, eukaryotes express a specialized UvrD family member, FBH1, which combines a helicase function with the ability to ubiquitylate target proteins. Previous results from analysis of *S. pombe*, mouse and human cells have indicated that the helicase activity of FBH1 is an important regulator of the function of RAD51. The data presented here indicate that RAD51 is also a substrate for the F-box-mediated E3 ubiquitin ligase action of FBH1.

Analysis of the FBH1-mediated ubiquitylation reaction suggests that RAD51 can be targeted on several lysine residues *in vitro*, although each protein is rarely modified more than once. The apparent monoubiquitylation of RAD51 generated by FBH1 is different from the polyubiquitylation events more usually seen with other SCF complexes. Among the five lysine residues being ubiquitylated *in vitro* by FBH1, some lie within domains of the protein that are critical for function. K58 is adjacent to E59, which is involved in the interaction with the BRC4 peptide of BRCA2 (ref. 33). Although we showed that the WT and K58/64R RAD51 proteins were equally effective at co-immunoprecipitating endogenous BRCA2, there is still a possibility that ubiquitylation of K58 might affect the RAD51–BRCA2 interaction under some circumstances. K64 has also been shown to be crucial in binding to both ssDNA and double-stranded DNA[34]. Similarly, K285 is a part of the ssDNA-binding loop 2 domain[35]. Ubiquitylation on K64 and K285 might, therefore, affect the RAD51–DNA interaction. In contrast, K156 lies within the ATPase core domain[35]. Ubiquitylation on K156 could possibly affect ATP binding and hydrolysis. The consequences of ubiquitylation on K107 remain unknown, as this residue does not seem to lie within any functional domain. We focused on analysis of two adjacent lysine residues in the non-catalytic N-terminal domain of RAD51, because the mass spectrometry data indicated that these were quantitatively by far the most important. Consistent with this, we found that the double K58/64R mutant was only very poorly ubiquitylated *in vitro* by the SCF^{FBH1} complex.

To define whether ubiquitylation of K58 and K64 of RAD51 plays a role in the regulation of RAD51's function in DNA repair

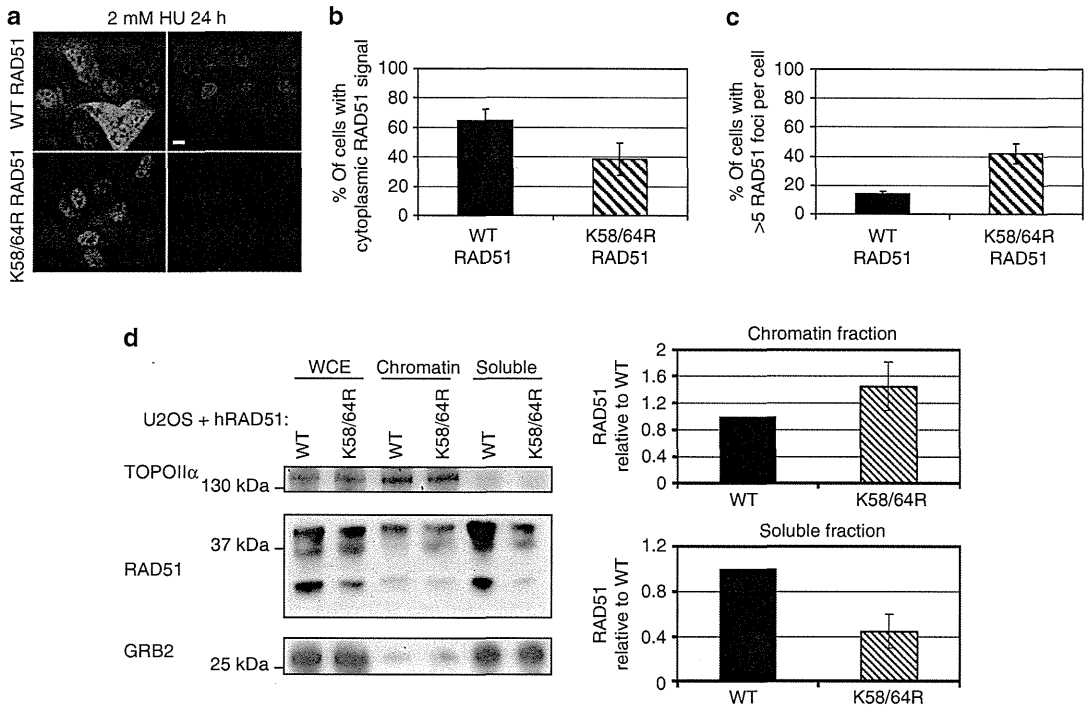

Figure 4 | Ubiquitylation of RAD51 regulates its intracellular localization. (**a**) Examples of RAD51 staining (green) in WT RAD51- and K58/64R RAD51-expressing cells after treatment with 2 mM HU for 24 h. Nuclei were stained with DAPI (blue). Scale bars, 10 μm (white). (**b**) The means of the percentage of cells showing cytoplasmic RAD51 staining are shown for three independent experiments. At least 50 cells for each cell line were quantified in each experiment. (**c**) The means of cells showing more than five RAD51 nuclear foci are shown for three independent experiments. At least 50 cells for each cell line were quantified in each experiment. (**d**) WT and K58/64R RAD51-expressing cells were exposed to 2 mM HU for 24 h. Whole-cell extracts (WCE), chromatin-bound proteins and soluble proteins were separated by SDS-PAGE and the samples were western blotted with an anti-TOPIIα antibody (a marker for chromatin bound proteins), an anti-RAD51 antibody, or an anti-GRB2 antibody (a marker for cytoplasmic proteins). In the right hand panels, the relative amount of RAD51 WT (black bars; set at 1 in each case) and K58/64R RAD51 (hatched bars) in the chromatin (upper) and soluble (lower) fractions were quantified by using ImageJ software. The means are shown for three independent experiments. Error bars represent s.d.

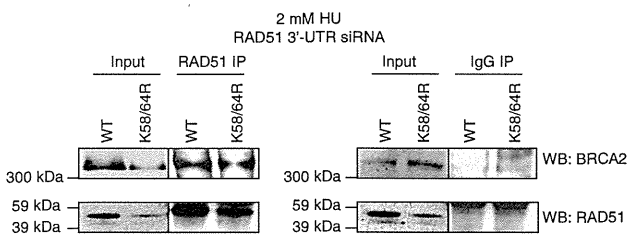

Figure 5 | RAD51 ubiquitylation does not disrupt the RAD51-BRCA2 interaction. WT RAD51- and K58/64R RAD51-expressing cells were treated with an siRNA targeting the 3'-UTR of RAD51 for 72 h, followed by a treatment with 2 mM HU for 24 h. Whole-cell extracts of WT RAD51- and K58/64R RAD51-expressing U2OS cells were incubated with anti-RAD51 (left panel) or anti-IgG control (right panel) antibodies. Precipitated proteins were separated by SDS-PAGE and the samples were western blotted with anti-BRCA2 and anti-RAD51 antibodies, as indicated.

or DNA replication, we compared the response of cells expressing either ectopic WT RAD51 or K58/64R RAD51 with a prolonged exposure to HU. We found several differences between these two transfected cell populations; most notably, the nuclear accumulation of K58/64R RAD51 was more prominent than it was with WT RAD51 following exposure to HU, and this was accompanied by enhanced HU resistance, a reduced level of HU-induced DSBs and hyperrecombination. These data support the model whereby ubiquitylation of RAD51 by FBH1 does not function to trigger RAD51 turnover by proteolysis, as is seen with several SCF-mediated ubiquitylation events, but rather serves to regulate the subcellular localization of RAD51. This suggests a potentially new paradigm for how SCF proteins can regulate target protein function. Nevertheless, our analyses would not detect the proteolytic removal of a small fraction of cellular RAD51 that exists, for example, at a very specific nuclear location. A previous study did observe that RAD51 is degraded via ubiquitylation, in a reaction that is regulated by RAD51C[36]. However, we found equivalent RAD51 protein levels in WT and K58/64R RAD51-expressing cells. On the other hand, it has also been reported that FBH1 is recruited to DNA replication and DNA damage sites by proliferating cell nuclear antigen (PCNA)[37]. Interestingly, FBH1 can itself be ubiquitylated (by $CRL4^{Cdt2}$), which leads to FBH1 degradation[37]. Moreover, ubiquitylation of FBH1 modulates its interaction with RAD51 (ref. 38). Therefore, the relationship between FBH1 and RAD51 is probably controlled by multiple ubiquitylation events.

There are a number of striking parallels between the phenotype of mammalian cells expressing the ubiquitylation-resistant form of RAD51 and those carrying a deletion in the helicase domain of FBH1. Our previous analysis of a mouse ES cell line with an internal deletion in the Fbh1 helicase domain showed that these cells are HU resistant, hyperrecombinogenic and less prone to accumulate DSBs following replication stress[23], all phenotypes reported here for the K58/64R RAD51-expressing cells. In the mouse mutant cells, RAD51 nuclear staining was prominent, even without exogenous DNA damage/replication blockade. In the

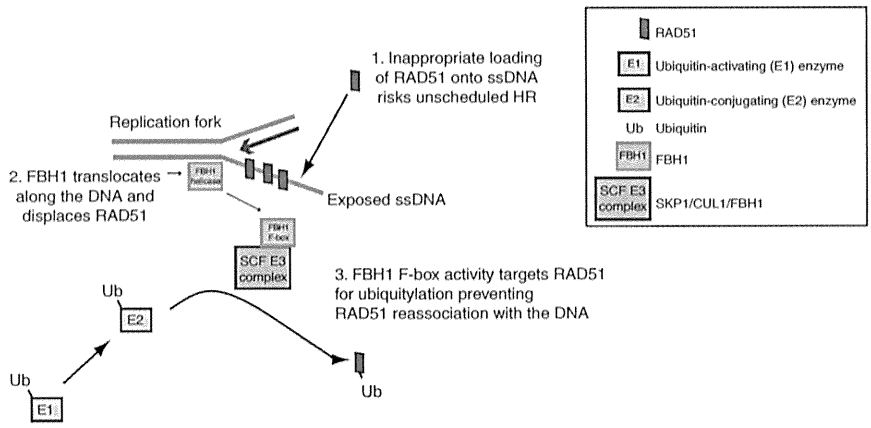

Figure 6 | Model for the proposed action of FBH1 at stalled DNA replication forks. Relevant proteins are shown, as indicated in the key. We propose that FBH1 translocates along DNA, where a physical interaction with RAD51 causes the dissociation of RAD51 from the developing nucleofilaments. Following this displacement of RAD51, the SCF^{FBH1} targets RAD51 for ubiquitylation, preventing its re-association with the DNA.

current work, the differences apparent following manipulation of the ubiquitylation status of RAD51 were only seen following replication stress. Nevertheless, the most straightforward explanation for these data is that the helicase and F-box functions of FBH1 operate together to regulate the same protein target or targets (see model in Fig. 6). Our data indicate that one key target in human cells is RAD51, but do not exclude the possibility that other targets for FBH1 exist. However, the fact that we can dominantly change the cellular response to HU simply by expressing a form of the proposed target protein that has altered ubiquitylation argues strongly that RAD51 is an important target for FBH1 during the cellular response to dNTP depletion and replication blockade. As ssDNA is commonly found adjacent to perturbed DNA replication sites, we tested the effect of ssDNA on the ubiquitylation reaction. Although we found that the presence of ssDNA does not alter the efficiency of the FBH1-mediated ubiquitylation reaction, it nevertheless might affect the specificity of the reaction *in vivo*.

Methods

Protein purification. *E. coli* expressing recombinant human RAD51 protein were lysed and sonicated in lysis buffer (0.1 M Tris-HCl pH 8, 2 mM EDTA, 5% glycerol, 0.5 mM dithiothreitol (DTT), 0.2 mg ml^{-1} phenylmethylsulfonyl fluoride and 0.1% Triton X-100). The soluble protein fraction was dialysed against spermidine buffer (20 mM Tris-acetate pH 7.5, 7 mM spermidine-NaOH and 0.1 mM DTT). Precipitates were collected and dissolved in P100 buffer (0.1 M potassium phosphate pH 6.8, 0.1 M KCl, 10% glycerol and 0.5 mM DTT) and were then loaded onto a hydroxyapatite column (Bio-Rad). Bound proteins were eluted with H buffer (0.1 M KCl, 10% glycerol and 0.5 mM DTT, containing a gradient of 0.1–0.8 M potassium phosphate pH 6.8). Fractions containing RAD51 were pooled and dialysed against R buffer (20 mM Tris-HCl pH 8, 1 mM EDTA, 0.5 mM DTT, 10% glycerol) containing 0.1 M KCl. Lysate was then loaded onto a heparin sepharose column (GE Healthcare) and eluted in R buffer with a linear gradient of 0.1–0.8 M KCl. Fractions containing RAD51 were again pooled and dialysed against R buffer containing 0.1 M KCl. Eluate was then loaded onto a mono-Q column (GE Healthcare) and eluted in R buffer with a linear gradient of 0.1–0.8 M KCl. Eluate was concentrated, dialysed against storage buffer (20 mM Tris-acetate pH 8, 0.2 M potassium acetate, 10% glycerol, 1 mM EDTA and 0.5 mM DTT) and stored at −80 °C[7].

S. cerevisiae expressing histidine-tagged human BLM protein were lysed in buffer A (50 mM HEPES-OH pH 7.2, 250 mM KCl, 10% glycerol and EDTA-free protease inhibitor (Roche)). The soluble protein fraction was subjected to nickel chelate affinity chromatography. The bound protein was eluted in buffer A containing 250 mM EDTA with an imidazole gradient of 50–1,500 mM. Fractions containing BLM were dialysed against buffer A containing 1 mM EDTA, 1 mM 2-mercaptoethanol and 0.1 mM phenylmethylsulfonyl fluoride, and stored at −80 °C[39]. Purified FANCD2 was a kind gift from Dr J.-Y. Masson. Purified RPA was a kind gift from Dr Pavel Janscak.

To purify the SCF^{FBH1} complex, the *FBH1* cDNA was obtained from an IMAGE clone library and was sub-cloned into pFastBac HT-A (Life Technologies, Inc.). The plasmid was then transformed into *E. coli* DH10Bac and recombinant bacmids were isolated for baculovirus preparation. Recombinant bacmids were transfected into SF21 cells to produce virus stocks. Baculoviruses encoding glutsthopne *S*-transferase (GST)-tagged SKP1, CUL1 and ROC1 were kindly provided by Dr Pavel Janscak. For SCF^{FBH1} complex production, SF21 cells were infected with the mixture of four recombinant baculoviruses: His-tagged FBH1, GST-tagged SKP1, and untagged CUL1 and ROC1, and the cells were incubated for 3 days. The infected SF21 cells were harvested and washed twice with ice-cold PBS. Cells were then lysed using lysis buffer (50 mM sodium phosphate buffer (pH7.4), 300 mM NaCl, 1 mM EDTA, 2 mM β-mercaptoethanol, 10% glycerol, 0.1% Nonidet P-40, Proteinase inhibitor complete (Roche)) for 1 h on ice. The lysate was clarified by centrifugation (Beckman, 70Ti, 70,000*g*, 4 °C, 1 h) and the supernatant was subsequently incubated with glutathione sepharose resin (GE healthcare) for 3 h. After the incubation, the resin was transferred to a disposable column (BioRad) and was washed with 20 bed volumes of GST-wash buffer (50 mM sodium phosphate buffer (pH7.4), 300 mM NaCl, 10% glycerol, 2 mM β-mercaptoethanol). Bound proteins were eluted using GST-elution buffer (50 mM sodium phosphate buffer (pH 7.4), 20 mM glutathione, 300 mM NaCl, 10% glycerol, 2 mM β-mercaptoethanol). The eluted fractions were incubated with Ni-NTA agarose (QIAGEN) overnight. The resin was transferred to a disposable column and was washed sequentially with HS wash buffer (50 mM sodium phosphate buffer (pH7.4), 500 mM NaCl, 10% glycerol, 1 mM β-mercaptoethanol, 10 mM imidazole) and IM wash buffer (50 mM sodium phosphate buffer (pH7.4), 300 mM NaCl, 10% glycerol, 1 mM β-mercaptoethanol, 25 mM imidazole). Bound proteins were eluted with HIS-elution buffer (50 mM sodium phosphate buffer (pH7.4), 300 mM NaCl, 10% glycerol, 1 mM β-mercaptoethanol, 300 mM imidazole). Aliquots were frozen in liquid N_2 and stored at −80 °C.

***In vitro* ubiquitylation assays.** A complete ubiquitylation reaction (10 μl), containing ubiquitylation buffer (50 mM HEPES-NaOH pH 7.5, 100 mM NaCl, 10 mM $MgCl_2$, 5 mM ATP, 0.1 mM DTT), 100 nM ubiquitin activating enzyme (Boston Biochem), 500 nM UbcH5a (Boston Biochem), 8 μM untagged or HA-tagged ubiquitin (Boston Biochem), 20 nM purified RAD51 and 5 ng μl^{-1} SCF^{FBH1}, was incubated at 37 °C for the indicated times. The reactions were terminated by incubation with 10 μl stop buffer (100 mM Tris-HCl pH 8, 5 mM EDTA pH 8.0, 0.2% SDS, 200 mM NaCl, 200 μg ml^{-1} proteinase K) at 65 °C for 15 min. The reaction products were analysed by SDS–PAGE followed by western blotting with antibodies against RAD51 (1:200, Abcam ab1837), BLM (1:1,000, Abcam ab476), FANCD2 (1:200, Santa Cruz sc28194), RPA14 (1:1,000, Tebu-bio GTX70238), RPA34 (1:1,000, Abcam ab2175) or RPA70 (1:1,000, NeoMarkers MS-692-P) using standard methods. Where indicated, 25 μg ml^{-1} ssDNA was included in the reaction. To test the ability of different E2 enzymes to support the ubiquitylation reaction, 500 nM Cdc34 or UbcH6 was used instead of UbcH5a. Cdc34 was also tested at the same concentration in combination with UbcH5, to assess whether this enhanced the reaction efficiency, as has been suggested previously[40]. Nedd8 (25 μM)- and Nedd8-activating enzyme (100 nM) were tested based on reports that SCF-mediated polyubiquitylation is activated by conjugation of Nedd8 to human CUL1 (refs 41,42), probably via conformational changes in CUL1 (ref. 43).

Immunoprecipitation of FBH1 and RAD51. Two hundred nanograms of GST (Santa Cruz) or GST-FBH1 was incubated with 4 pmol WT or K58/64R RAD51 in 500 μl binding buffer (10 mM Tris-HCl pH8, 150 mM NaCl, 1 mM EDTA and 0.2% TrintonX-100) at 4 °C for 15 min. Forty microlitres of Glutathione Sepharose (GE Healthcare) was added and the protein mixture was incubated at 4 °C for 1 h.

The sepharose was collected and washed with the binding buffer five times. The sepharose was then boiled with the sample buffer (0.4% SDS, 2% glycerol, 12 mM Tris-HCl pH 6.8, 0.1% (w/v) bromophenol blue, 5% (w/v) β-mercaptoethanol) and the released proteins were analysed by using western blotting. Membranes were probed with antibodies against GST (1:200, Santa Cruz sc138) or RAD51 (1:1,000, Santa Cruz sc8349).

Mass spectrometry-based analysis of RAD51 ubiquitylation. Proteins were resolved by SDS–PAGE, followed by in-gel digestion with trypsin. Peptide fractions were analysed on a Orbitrap mass spectrometer (Velos, Thermo Scientific) equipped with a nanoflow HPLC system (Thermo Scientific) using a data-dependent method, dynamically choosing the ten most abundant precursor ions from the survey scan for higher energy collisional dissociation fragmentation. Survey scans were acquired at a resolution of 30,000 at *m/z* 400, while the resolution for higher energy collisional dissociation spectra was set to 7,500 at *m/z* 400 (ref. 44). Raw data files were analysed using MaxQuant software (version 1.2.2.9)[45].

Cell culture. Human U2OS cells (obtained from the ATCC) were maintained in DMEM medium supplemented with 10% FCS and 2.4 mM glutamine. Cells were grown at 37 °C in a humidified atmosphere containing 5% CO_2. Cells were transfected with plasmids expressing WT or mutated RAD51 under the control of cytomegalovirus promoter in vector pcDNA3 (a gift from Dr Fiona Benson) using standard techniques. Where indicated, cells were transfected with control siRNA (5′-UCUGUCGUUAGUGUCACCGGUCAUA-3′) or siRNA targeting the 3′-UTR of the *RAD51* gene (5′-UCUUCCUGUUGUG ACUGCCAGGAUA-3′) for 72 h before HU treatment. To target the coding region of RAD51, the following siRNA was used: 5′-GCGACUCGCUGAUGAGUUUTT-3′. As a control, an siRNA with the following sequence was used: 5′-GCGGCUGUCG UAGAACUUUTT-3′.

Pulsed-field gel electrophoresis. Cells were treated with 2 mM HU for various times. After treatment, 10^6 cells were embedded into 0.9% agarose gel plugs using a CHEF disposable plug mould (BioRad). The plugs were incubated in lysis buffer (100 mM EDTA, 1% sodium lauryl sarcosine, 0.2% sodium deoxycholate, 1 mg ml^{-1} proteinase K) for 2 days and run in an 0.9% agarose gel using a Rotaphor apparatus (Biometra)[46]. The gel was then stained with ethidium bromide and the DNA was analysed using a Typhoon 9200 scanner (Amersham). Band intensities were quantified using ImageQuant 5.2 software. All experiments were performed at least three times.

Clonogenic survival assays. Cells were incubated in HU or Aphidicolin-containing medium for 24 h. After treatment, cells were washed with PBS and then grown in fresh medium for 8–10 days. Colonies were fixed, stained and counted using Coomassie solution (0.1% Coomassie Blue, 7% acetic acid, 50% methanol). All experiments were performed at least three times.

DR-GFP recombination assay. The recombination level in U2OS cells was measured by transfecting cells using electroporation (Gene Pulser Xcell, Bio-Rad) with the DSB recombination reporter (which generates an intact GFP gene following recombination) and an I-*Sce*I endonuclease expression vector. A red fluorescent protein expression vector was used as a control, to define transfection efficiency. Cells were analysed by flow cytometry for green/red fluorescence 3 days after transfection[28].

Immunofluorescence analysis. Cells in DMEM medium were seeded onto glass coverslips at ~25% confluency. Twenty-four hours later, the cells were treated with 2 mM HU and were then incubated at 37 °C for 24 h. Cells were then fixed in 4% *para*-formaldehyde in PBS for 10 min, washed in PBS and were stored at 4 °C. After permeabilization with 0.1% TritonX-100 in PBS, the cells were washed in freshly made blocking buffer (0.15% glycine (w/v), 0.5% BSA (w/v) in PBS). Staining with primary antibody against RAD51 (1:200, Santa Cruz sc8349) was followed by further washes with 0.1% TritonX-100 in PBS and then incubation with secondary antibody conjugated with AF488 (1:800, Invitrogen A21206). The nuclei were counterstained with DAPI (Vector Laboratories) before the coverslips were sealed to glass slides. RAD51 staining patterns were visualized with a confocal laser scanning microscope (Zeiss LSM 710) and images were stored and analysed using Zeiss LSM Image Browser software.

Separation of soluble and chromatin-associated proteins. Cells were treated with 2 mM HU and incubated at 37 °C for 24 h. A pellet of ~2×10^6 cells was washed three times in PBS and then re-suspended in 250 μl freshly made protein buffer A (10 mM HEPES, 10 mM KCl, 1.5 mM $MgCl_2$, 0.34 M sucrose, 10% glycerol, 1 mM DTT, 0.1% TritonX-100, protease inhibitor complete (Roche)) for 1 h at 4 °C. The sample was centrifuged at 200*g* for 4 min at 4 °C and the supernatant was stored as the cytoplasmic soluble fraction. The pellet was washed three times in 200 μl Protein Buffer A, centrifuged at 180*g* for 4 min at 4 °C before addition of 175 μl of freshly made protein buffer B (3 mM EDTA, 0.2 mM EGTA, 1 mM DTT, protease inhibitor complete (Roche)). Incubation continued for 1 h at 4 °C, followed by centrifugation at 300 *g* for 4 min at 4 °C. The supernatant was stored as the nuclear soluble fraction. The pellet was washed three times in 175 μl Protein Buffer B, centrifuged at 16,000*g* for 1 min at 4 °C before the supernatant was discarded, and the pellet (chromatin-associated fraction) was resuspended and boiled in 175 μl Laemmli buffer (0.4% SDS, 2% glycerol, 12 mM Tris-HCl pH 6.8). For western blotting analysis, 10 × BFB-2-ME (0.1% (w/v) bromophenol blue, 5% (w/v) β-mercaptoethanol) was added, the samples were boiled, and the cytoplasmic and nuclear soluble fractions were combined. Membranes were probed with antibodies against RAD51 (1:1,000, Abcam ab1837), TOPOIIα (1:1,000, Santa Cruz sc5347) or GRB2 (1:1,000, BD Transduction lab 610112). Uncropped gel scans can be found in Supplementary Fig. 5.

DNA fibre analysis. U2OS cells were pulse-labelled with 50 μM CldU for 20 min. The cells were rinsed with fresh medium and were incubated with 2 mM HU for 24 h. Cells were rinsed with medium again and pulse labelled with 500 μM IdU for 1 h. For untreated cells, the HU incubation was omitted. Labelled cells were harvested and DNA fibres were spread on glass slides[47]. DNA fibres were denatured with 2.5 M hydrochloric acid for 90 min and then rinsed with freshly made blocking buffer (0.15% glycine (w/v), 0.5% BSA (w/v) in PBS). CldU and IdU were detected by incubating slides with primary antibodies (1:40, Abcam ab6326 and 1:2, Becton Dickinson 347580, respectively). DNA fibres were washed with blocking buffer again, and then incubated with secondary antibodies conjugated with AF568 (1:200, Invitrogen A11077) or AF488 (1:200, Invitrogen A21200). At least 180 replication structures for each analysis were scored using a Nikon Eclipse 80i microscope equipped with ACT-1 software.

Immunoprecipitation of RAD51 and BRCA2. Cells were treated with 2 mM HU and incubated at 37 °C for 24 h. Cells were washed three times in cold PBS and then scraped in 1 ml RIPA buffer (50 mM Tris pH 7.5, 150 mM NaCl, 1% TrintonX-100, 0.1% sodium deoxycholate, 1 mM EDTA, 5 mM β-glycerophosphate, 1 mM sodium orthovanadate and 5 mM sodium fluoride, protease inhibitor complete (Roche)). Cells were lysed in RIPA buffer at 4 °C for 30 min. The lysate was sonicated briefly and then incubated with RAD51 antibody (1:40, Santa Cruz sc8349) or rabbit IgG antibody (1:80, Santa Cruz sc2027) at 4 °C for 1 h. Twenty-five microlitres of protein G Sepharose (Invitrogen) was added to the lysate and incubated at 4 °C for 1 h. The sepharose was collected and washed with the RIPA buffer three times. The sepharose was then boiled with the sample buffer (0.4% SDS, 2% glycerol, 12 mM Tris-HCl pH 6.8, 0.1% (w/v) bromophenol blue, 5% (w/v) β-mercaptoethanol) and analysed by using western blotting. Membranes were probed with antibodies against BRCA2 (1:1,000, Abcam ab123491) or RAD51 (1:1,000, Santa Cruz sc8349).

References

1. Petermann, E. & Helleday, T. Pathways of mammalian replication fork restart. *Nat. Rev. Mol. Cell. Biol.* **11,** 683–687 (2010).
2. Hanada, K. *et al.* The structure-specific endonuclease Mus81 contributes to replication restart by generating double-strand DNA breaks. *Nat. Struct. Mol. Biol.* **14,** 1096–1104 (2007).
3. Petermann, E., Orta, M. L., Issaeva, N., Schultz, N. & Helleday, T. Hydroxyurea-stalled replication forks become progressively inactivated and require two different RAD51-mediated pathways for restart and repair. *Mol. Cell* **37,** 492–502 (2010).
4. Robu, M. E., Inman, R. B. & Cox, M. M. RecA protein promotes the regression of stalled replication forks in vitro. *Proc. Natl Acad. Sci. USA* **98,** 8211–8218 (2001).
5. Hashimoto, Y., Ray Chaudhuri, A., Lopes, M. & Costanzo, V. Rad51 protects nascent DNA from Mre11-dependent degradation and promotes continuous DNA synthesis. *Nat. Struct. Mol. Biol.* **17,** 1305–1311 (2010).
6. Schlacher, K. *et al.* Double-strand break repair-independent role for BRCA2 in blocking stalled replication fork degradation by MRE11. *Cell* **145,** 529–542 (2011).
7. Benson, F. E., Stasiak, A. & West, S. C. Purification and characterization of the human Rad51 protein, an analogue of *E. coli* RecA. *EMBO J.* **13,** 5764–5771 (1994).
8. Hashimoto, Y., Puddu, F. & Costanzo, V. RAD51- and MRE11-dependent reassembly of uncoupled CMG helicase complex at collapsed replication forks. *Nat. Struct. Mol. Biol.* **19,** 17–24 (2011).
9. Luo, G. *et al.* Cancer predisposition caused by elevated mitotic recombination in Bloom mice. *Nat. Genet.* **26,** 424–429 (2000).
10. Bugreev, D. V., Yu, X., Egelman, E. H. & Mazin, A. V. Novel pro- and anti-recombination activities of the Bloom's syndrome helicase. *Genes Dev.* **21,** 3085–3094 (2007).
11. Hu, Y. *et al.* RECQL5/Recql5 helicase regulates homologous recombination and suppresses tumor formation via disruption of Rad51 presynaptic filaments. *Genes Dev.* **21,** 3073–3084 (2007).
12. Veaute, X. *et al.* The Srs2 helicase prevents recombination by disrupting Rad51 nucleoprotein filaments. *Nature* **423,** 309–312 (2003).
13. Krejci, L. *et al.* DNA helicase Srs2 disrupts the Rad51 presynaptic filament. *Nature* **423,** 305–309 (2003).

14. Moldovan, G. L. *et al.* Inhibition of homologous recombination by the PCNA-interacting protein PARI. *Mol. Cell* **45,** 75–86 (2011).
15. Fugger, K. *et al.* Human Fbh1 helicase contributes to genome maintenance via pro- and anti-recombinase activities. *J. Cell Biol.* **186,** 655–663 (2009).
16. Chiolo, I. *et al.* The human F-Box DNA helicase FBH1 faces *Saccharomyces cerevisiae* Srs2 and postreplication repair pathway roles. *Mol. Cell. Biol.* **27,** 7439–7450 (2007).
17. Cardozo, T. & Pagano, M. The SCF ubiquitin ligase: insights into a molecular machine. *Nat. Rev. Mol. Cell. Biol.* **5,** 739–751 (2004).
18. Osman, F., Dixon, J., Barr, A. R. & Whitby, M. C. The F-Box DNA helicase Fbh1 prevents Rhp51-dependent recombination without mediator proteins. *Mol. Cell. Biol.* **25,** 8084–8096 (2005).
19. Sakaguchi, C., Morishita, T., Shinagawa, H. & Hishida, T. Essential and distinct roles of the F-box and helicase domains of Fbh1 in DNA damage repair. *BMC Mol. Biol.* **9,** 27 (2008).
20. Morishita, T. *et al.* Role of the *Schizosaccharomyces pombe* F-Box DNA helicase in processing recombination intermediates. *Mol. Cell. Biol.* **25,** 8074–8083 (2005).
21. Lorenz, A., Osman, F., Folkyte, V., Sofueva, S. & Whitby, M. C. Fbh1 limits Rad51-dependent recombination at blocked replication forks. *Mol. Cell. Biol.* **29,** 4742–4756 (2009).
22. Simandlova, J. *et al.* FBH1 helicase disrupts RAD51 filaments *in vitro* and modulates homologous recombination in mammalian cells. *J. Biol. Chem.* **288,** 34168–34180 (2013).
23. Fugger, K. *et al.* FBH1 co-operates with MUS81 in inducing DNA double-strand breaks and cell death following replication stress. *Nat. Commun.* **4,** 1423 (2013).
24. Jeong, Y. T., Cermak, L., Guijarro, M. V., Hernando, E. & Pagano, M. FBH1 protects melanocytes from transformation and is deregulated in melanomas. *Cell Cycle* **12,** 1128–1132 (2013).
25. Jeong, Y. T. *et al.* FBH1 promotes DNA double-strand breakage and apoptosis in response to DNA replication stress. *J. Cell Biol.* **200,** 141–149 (2013).
26. Wagner, S. A. *et al.* A proteome-wide, quantitative survey of in vivo ubiquitylation sites reveals widespread regulatory roles. *Mol. Cell. Proteomics* **10,** M111 013284 (2011).
27. Raderschall, E. *et al.* Formation of higher-order nuclear Rad51 structures is functionally linked to p21 expression and protection from DNA damage-induced apoptosis. *J. Cell. Sci.* **115,** 153–164 (2002).
28. Nakanishi, K., Cavallo, F., Brunet, E. & Jasin, M. Homologous recombination assay for interstrand cross-link repair. *Methods Mol. Biol.* **745,** 283–291 (2011).
29. Wong, A. K., Pero, R., Ormonde, P. A., Tavtigian, S. V. & Bartel, P. L. RAD51 interacts with the evolutionarily conserved BRC motifs in the human breast cancer susceptibility gene brca2. *J. Biol. Chem.* **272,** 31941–31944 (1997).
30. Jensen, R. B., Carreira, A. & Kowalczykowski, S. C. Purified human BRCA2 stimulates RAD51-mediated recombination. *Nature* **467,** 678–683 (2010).
31. Liu, J., Doty, T., Gibson, B. & Heyer, W. D. Human BRCA2 protein promotes RAD51 filament formation on RPA-covered single-stranded DNA. *Nat. Struct. Mol. Biol.* **17,** 1260–1262 (2010).
32. Thorslund, T. *et al.* The breast cancer tumor suppressor BRCA2 promotes the specific targeting of RAD51 to single-stranded DNA. *Nat. Struct. Mol. Biol.* **17,** 1263–1265 (2010).
33. Subramanyam, S., Jones, W. T., Spies, M. & Spies, M. A. Contributions of the RAD51 N-terminal domain to BRCA2-RAD51 interaction. *Nucleic Acids Res.* **41,** 9020–9032 (2013).
34. Aihara, H., Ito, Y., Kurumizaka, H., Yokoyama, S. & Shibata, T. The N-terminal domain of the human Rad51 protein binds DNA: structure and a DNA binding surface as revealed by NMR. *J. Mol. Biol.* **290,** 495–504 (1999).
35. Prasad, T. K., Yeykal, C. C. & Greene, E. C. Visualizing the assembly of human Rad51 filaments on double-stranded DNA. *J. Mol. Biol.* **363,** 713–728 (2006).
36. Bennett, B. T. & Knight, K. L. Cellular localization of human Rad51C and regulation of ubiquitin-mediated proteolysis of Rad51. *J. Cell. Biochem.* **96,** 1095–1109 (2005).
37. Bacquin, A. *et al.* The helicase FBH1 is tightly regulated by PCNA via CRL4(Cdt2)-mediated proteolysis in human cells. *Nucleic Acids Res.* **41,** 6501–6513 (2013).
38. Masuda-Ozawa, T., Hoang, T., Seo, Y. S., Chen, L. F. & Spies, M. Single-molecule sorting reveals how ubiquitylation affects substrate recognition and activities of FBH1 helicase. *Nucleic Acids Res.* **41,** 3576–3587 (2013).
39. Karow, J. K., Newman, R. H., Freemont, P. S. & Hickson, I. D. Oligomeric ring structure of the Bloom's syndrome helicase. *Curr. Biol.* **9,** 597–600 (1999).
40. Fong, P. C. *et al.* Inhibition of poly(ADP-ribose) polymerase in tumors from BRCA mutation carriers. *N. Engl. J. Med.* **361,** 123–134 (2009).
41. Pan, Z. Q., Kentsis, A., Dias, D. C., Yamoah, K. & Wu, K. Nedd8 on cullin: building an expressway to protein destruction. *Oncogene* **23,** 1985–1997 (2004).
42. Saha, A. & Deshaies, R. J. Multimodal activation of the ubiquitin ligase SCF by Nedd8 conjugation. *Mol. Cell* **32,** 21–31 (2008).
43. Duda, D. M. *et al.* Structural insights into NEDD8 activation of cullin-RING ligases: conformational control of conjugation. *Cell* **134,** 995–1006 (2008).
44. Michalski, A. *et al.* Mass spectrometry-based proteomics using Q Exactive, a high-performance benchtop quadrupole Orbitrap mass spectrometer. *Mol. Cell. Proteomics* **10,** M111 011015 (2011).
45. Cox, J. & Mann, M. MaxQuant enables high peptide identification rates, individualized p.p.b.-range mass accuracies and proteome-wide protein quantification. *Nat. Biotechnol.* **26,** 1367–1372 (2008).
46. Hanada, K. *et al.* The structure-specific endonuclease Mus81-Eme1 promotes conversion of interstrand DNA crosslinks into double-strands breaks. *EMBO J.* **25,** 4921–4932 (2006).
47. Jackson, D. A. & Pombo, A. Replicon clusters are stable units of chromosome structure: evidence that nuclear organization contributes to the efficient activation and propagation of S phase in human cells. *J. Cell Biol.* **140,** 1285–1295 (1998).
48. Flygare, J., Armstrong, R. C., Wennborg, A., Orsan, S. & Hellgren, D. Proteolytic cleavage of HsRad51 during apoptosis. *FEBS Lett.* **427,** 247–251 (1998).

Acknowledgements

We thank members of the Hickson laboratory for useful discussions, Drs Y. Liu and H.W. Mankouri for critical reading of the manuscript, and The Nordea Foundation, Cancer Research UK, The Association for International Cancer Research, The Danish Medical Research Council, The European Research Council and The Danish Cancer Society for financial support.

Author contributions

W.K.C., M.J.P., P.B. and K.H. designed and performed experiments, and analysed data. C.C. and I.D.H. designed experiments and analysed data. W.K.C. and I.D.H. wrote the manuscript.

Additional information

Supplementary Information accompanies this paper at http://www.nature.com/naturecommunications

Competing financial interests: The authors declare no competing financial interests.

Reprints and permission information is available online at http://npg.nature.com/reprintsandpermissions/

How to cite this article: Chu, W. K. *et al.* FBH1 influences DNA replication fork stability and homologous recombination through ubiquitylation of RAD51. *Nat. Commun.* 6:5931 doi: 10.1038/ncomms6931 (2015).

Leukemia (2014) **28**, 1586–1595

www.nature.com/leu

ORIGINAL ARTICLE

Comprehensive analysis of genetic alterations and their prognostic impacts in adult acute myeloid leukemia patients

R Kihara[1,27], Y Nagata[2,3,27], H Kiyoi[1], T Kato[1], E Yamamoto[1], K Suzuki[1], F Chen[1], N Asou[4], S Ohtake[5], S Miyawaki[6], Y Miyazaki[7], T Sakura[8], Y Ozawa[9], N Usui[10], H Kanamori[11], T Kiguchi[12], K Imai[13], N Uike[14], F Kimura[15], K Kitamura[16], C Nakaseko[17], M Onizuka[18], A Takeshita[19], F Ishida[20], H Suzushima[21], Y Kato[22], H Miwa[23], Y Shiraishi[24], K Chiba[24], H Tanaka[25], S Miyano[24,25], S Ogawa[2,3] and T Naoe[1,26]

To clarify the cooperative roles of recurrently identified mutations and to establish a more precise risk classification system in acute myeloid leukemia (AML), we comprehensively analyzed mutations in 51 genes, as well as cytogenetics and 11 chimeric transcripts, in 197 adult patients with *de novo* AML who were registered in the Japan Adult Leukemia Study Group AML201 study. We identified a total of 505 mutations in 44 genes, while only five genes, *FLT3*, *NPM1*, *CEBPA*, *DNMT3A* and *KIT*, were mutated in more than 10% of the patients. Although several cooperative and exclusive mutation patterns were observed, the accumulated mutation number was higher in cytogenetically normal AML and lower in AML with *RUNX1-RUNX1T1* and *CBFB-MYH11*, indicating a strong potential of these translocations for the initiation of AML. Furthermore, we evaluated the prognostic impacts of each sole mutation and the combinations of mutations and/or cytogenetics, and demonstrated that AML patients could be clearly stratified into five risk groups for overall survival by including the mutation status of *DNMT3A*, *MLL*-PTD and *TP53* genes in the risk classification system of the European LeukemiaNet. These results indicate that the prognosis of AML could be stratified by the major mutation status in combination with cytogenetics.

Leukemia (2014) **28** 1586–1595; doi:10.1038/leu.2014.55

Keywords: acute myeloid leukemia; gene mutations; prognosis; risk factor

INTRODUCTION

Acute myeloid leukemia (AML) is a clinically and genetically heterogeneous disease.[1,2] Although about 80% of younger adults with AML achieve complete remission (CR) with induction chemotherapy, more than half of the CR patients relapse, even if they receive intensive consolidation therapies. Allogeneic hematopoietic stem cell transplantation (allo-SCT) is applied to the patients who have risk factors for relapse, and it has been demonstrated by meta-analysis that allo-SCT at the first CR improves the long-term prognosis of the cytogenetically intermediate- and adverse-risk groups.[3] Cytogenetic-risk classification for AML is well established and commonly used as criteria for the application of allo-SCT at the first CR, whereas there is clinical heterogeneity in the intermediate-risk group, particularly cytogenetically normal (CN)-AML.[4] Recent advances and the accumulation of information on the prognostic relevance of recurrent genetic alterations have made more detailed risk stratification possible in AML patients.[5–19] The European LeukemiaNet (ELN) has recommended a novel risk classification system on the basis of the cytogenetic and genetic status.[2] In this system, CN-AML is stratified into two risk groups according to the mutation status of *FLT3*, *NPM1* and *CEBPA*: patients with *NPM1* mutation but not *FLT3*-ITD and those with *CEBPA* mutation are included in the favorable-risk (FR) group, and patients with *FLT3*-ITD and those with neither *NPM1* mutation nor *FLT3*-ITD are categorized into the intermediate-I-risk (IR-I) group. Long-term prognosis according to the ELN classification system was retrospectively evaluated in well-established cohorts, and it has

[1]Department of Hematology and Oncology, Nagoya University Graduate School of Medicine, Nagoya, Japan; [2]Cancer Genomics Project, Graduate School of Medicine, The University of Tokyo, Tokyo, Japan; [3]Department of Pathology and Tumor Biology, Graduate School of Medicine, Kyoto University, Kyoto, Japan; [4]Department of Hematology, Kumamoto University School of Medicine, Kumamoto, Japan; [5]Department of Clinical Laboratory Science, Kanazawa University Graduate School of Medical Sciences, Kanazawa, Japan; [6]Division of Hematology, Tokyo Metropolitan Ohtsuka Hospital, Tokyo, Japan; [7]Department of Hematology, Atomic Bomb Disease Institute, Nagasaki University Graduate School of Biomedical Sciences, Nagasaki, Japan; [8]Leukemia Research Center, Saiseikai Maebashi Hospital, Maebashi, Japan; [9]Department of Hematology, Japanese Red Cross Nagoya First Hospital, Nagoya, Japan; [10]Division of Clinical Oncology and Hematology, Department of Internal Medicine, Jikei University School of Medicine, Tokyo, Japan; [11]Department of Hematology, Kanagawa Cancer Center, Kanagawa, Japan; [12]Department of Hematology, Tokyo Medical University, Tokyo, Japan; [13]Department of Hematology, Sapporo Hokuyu Hospital, Sapporo, Japan; [14]Department of Hematology, National Hospital Organization Kyushu Cancer Center, Fukuoka, Japan; [15]Division of Hematology, Department of Internal Medicine, National Defense Medical College, Saitama, Japan; [16]Division of Hematology, Ichinomiya Municipal Hospital, Ichinomiya, Japan; [17]Department of Hematology, Chiba University Hospital, Chiba, Japan; [18]Department of Hematology and Oncology, Tokai University School of Medicine, Isehara, Japan; [19]Department of Internal Medicine, Hamamatsu University School of Medicine, Hamamatsu, Japan; [20]Division of Hematology, Department of Internal Medicine, Shinshu University School of Medicine, Matsumoto, Japan; [21]Department of Hematology, Kumamoto Shinto General Hospital, Kumamoto, Japan; [22]Department of Neurology, Hematology, Metabolism, Endocrinology, and Diabetology (DNHMED), Yamagata University School of Medicine, Yamagata, Japan; [23]Department of Internal Medicine, Division of Hematology, Aichi Medical University School of Medicine, Nagakute, Japan; [24]Laboratory of DNA Information Analysis, Human Genome Center, The Institute of Medical Science, The University of Tokyo, Tokyo, Japan; [25]Laboratory of Sequence Analysis, Human Genome Center, The Institute of Medical Science, The University of Tokyo, Tokyo, Japan and [26]National Hospital Organization Nagoya Medical Center, Nagoya, Japan. Correspondence: Dr H Kiyoi, Department of Hematology and Oncology, Nagoya University Graduate School of Medicine, Tsurumai-cho 65, Showa-ku, Nagoya, Aichi 466-8550, Japan or Professor S Ogawa, Department of Pathology and Tumor Biology, Graduate School of Medicine, Kyoto University, Kyoto, Japan.
E-mail: kiyoi@med.nagoya-u.ac.jp or sogawa-tky@umin.ac.jp
[27]These authors contributed equally to this work.
Received 3 December 2013; revised 21 January 2014; accepted 24 January 2014; accepted article preview online 3 February 2014; advance online publication, 14 February 2014